

Starvation suppression in scale-free metabolic networks: Dynamical mean-field analysis of dense catalytic reaction networks

Kota Mitsumoto^{1,*} and Shuji Ishihara^{1,2,†}

¹*Graduate School of Arts and Sciences, University of Tokyo,
Komaba 3-8-1, Meguro-ku, Tokyo 153-8902, Japan*

²*Universal Biology Institute, University of Tokyo,
Komaba 3-8-1, Meguro-ku, Tokyo 153-8902, Japan*

(Dated: March 23, 2026)

Cellular metabolic networks exhibit scale-free topologies with power-law degree distributions across diverse organisms. Although such topologies are often linked to mutational robustness and evolutionary advantage, their role in metabolic dynamics remains unclear. Using dynamical mean-field theory, we derive an exact solution for an intracellular catalytic reaction model on dense random networks with arbitrary degree distributions. We show that the metabolic-starvation transition observed under nutrient-poor conditions for homogeneous degree distributions disappears when the out-degree distribution is scale-free. We also show that the power-law distribution of biomolecular abundances observed in real cells reflects the power-law in-degree distribution of the underlying catalytic reaction network. Large-scale numerical simulations validate these predictions. Our results provide a theoretical framework linking network topology and metabolic dynamics, and identify a dynamical advantage of scale-free topology under nutrient limitation.

I. INTRODUCTION

Living systems sustain diverse vital functions through their intrinsic complexity [1–3]. Even a single cell maintains metabolism through a rich mixture of chemical species interacting within highly interconnected reaction networks [4–8]. Network science has revealed that such metabolic networks are not completely random but exhibit characteristic structural organization [9–11]. In particular, many metabolic networks possess a scale-free topology, characterized by power-law degree distributions and the presence of a few highly connected hubs [12–18]. This topology is widely observed across diverse complex systems, including social [19, 20], technological [21, 22], and information networks [23, 24]. Scale-free networks exhibit remarkable robustness to the random removal of nodes or edges [25–29], corresponding to mutational robustness in biological systems. The possible evolutionary advantages associated with this robustness have been discussed [30, 31]. However, how the scale-free topology influences the dynamical behavior of metabolic systems remains poorly understood.

Scale-free networks are known to influence macroscopic dynamical states [9, 11, 32–34], often eliminating phase transitions, as seen in the ferromagnetic Ising model [35] and epidemic spreading models [36]. In these systems, hubs effectively couple a large fraction of nodes and thereby promote global ordering. This raises the question of whether similar effects occur in biological systems. Metabolic networks also exhibit qualitative changes in cellular states, including transitions between living and non-living states [37, 38] and cell differentiation [39, 40].

However, it remains unclear how the scale-free topology of metabolic networks influences these transitions, for example, in helping cells avoid death or starvation. Another important universal feature of cellular systems is the distribution of biomolecular abundances, including those of mRNAs and metabolites, which often follows a power-law [41–45]. The relationship between this statistical feature and the scale-free topology of metabolic networks also remains largely unclear.

To unravel the impact of scale-free topology on metabolic dynamics, we analyze a minimal model that captures essential mechanisms while abstracting away microscopic details. A simple catalytic reaction network model incorporating cell growth and nutrient uptake was introduced by Furusawa and Kaneko (see Fig. 1(a)) [41, 46–48]. The model has succeeded in capturing power-law distributions in both biomolecular abundances and network degrees via evolutionary selection with higher cellular growth rates [47]. However, the contribution of the power-law degree distribution to the high cellular growth rate and the biomolecular abundance distribution remains unclear, partly due to the lack of exact analytical results beyond numerical simulations. To address this issue, it is useful to analyze random network models in the limits of large system size and dense connectivity. In these limits, an exact analytical treatment becomes possible using dynamical mean-field theory (DMFT) [49–55], which is based on a generating-functional formalism for dynamical paths and enables ensemble averaging over random network topologies. Furthermore, recent technical developments extend this framework to networks with arbitrary degree distributions [56–58], thereby allowing systematic comparisons among networks with different degrees of connectivity heterogeneity, as displayed in Fig. 1(b).

In this paper, we analyze a densely connected catalytic reaction network model using DMFT. We derive

* kmitsumoto@g.ecc.u-tokyo.ac.jp

† csishihara@g.ecc.u-tokyo.ac.jp

exact effective dynamical equations conditioned on in- and out-degrees and obtain their fixed points for arbitrary degree distributions. We show that the model exhibits three states: metabolic, overnutrition, and starvation states. The transition between metabolic and overnutrition states occurs under high nutrient supply via a transcritical bifurcation, and the phase boundary is independent of both in- and out-degree distribution. On the other hand, the boundary of the metabolic-starvation transition, which occurs under low nutrient supply, is highly sensitive to the out-degree distribution. In particular, the transition to the starvation state disappears for power-law out-degree distributions. Furthermore, we find that the effect of connectivity heterogeneity reverses depending on nutrient availability: under nutrient-rich conditions, larger heterogeneity suppresses the growth rate, whereas under nutrient-poor conditions it enhances growth and prevents the starvation state. This implies that scale-free networks can provide an advantage in nutrient-poor environments. In addition, we verify the validity of the dense-limit results by comparing with numerical simulations on Erdős-Rényi (ER) networks [11, 32, 59] and one of scale-free networks called directed Barabási-Albert (dBA) networks [11, 60] with finite connectivity c (see Appendix A for numerical methods), and find the quantitative agreements down to $c \approx 10$. Finally, we show that a power-law in-degree distribution yields a power-law tail in the abundance distribution of biomolecules. This prediction is also confirmed by numerical simulations on dBA networks.

II. MODEL

We adopt the model used in [41, 47, 48], in which a cell is represented as a membrane-bound compartment containing N chemical species that interact through catalytic reactions on a random network, as illustrated in Fig. 1(a). The abundance of each chemical species is denoted by $x_i(t)$ for $i = 1, 2, \dots, N$. The catalytic reactions in this model take the simple form $j + k \rightarrow i + k$, representing the conversion of the chemical species j into i , catalyzed by k . In this reaction, the production rate of x_i and consumption rate of x_j are both given by $x_j x_k$, thereby the total abundance $x_i + x_j$ is conserved. The chemical species are divided into three groups: unpenetrable metabolic products, penetrable metabolic products, and nutrients, denoted by $\mathcal{G}_1, \mathcal{G}_2$ and \mathcal{G}_3 , respectively. The fraction of chemical species in \mathcal{G}_n is denoted by α_n , satisfying $\alpha_1 + \alpha_2 + \alpha_3 = 1$. Nutrients are assumed to be catalytically inactive. Penetrable metabolic products and nutrients can pass through the membrane and exchange with the external environment at rates $-dx_i$ and $d(g - x_i)$, respectively, where d is the membrane permeability, and g is the equilibrium abundance of nutrients in the environment. For convenience, we introduce parameters (d_i, g_i) , defined as $(0, 0)$ for $i \in \mathcal{G}_1$, $(d, 0)$ for $i \in \mathcal{G}_2$, and (d, g) for $i \in \mathcal{G}_3$. The cell grows by tak-

ing up nutrients from the environment; accordingly, the abundances of chemical species are uniformly diluted by $-\mu x_i$, where $\mu = \frac{1}{N} \sum_{i=1}^N d_i (g_i - x_i)$ is the cell growth rate.

Taken together, the dynamics of $x_i(t)$ is governed by the following equations:

$$\begin{aligned} \dot{x}_i(t) = & \frac{1}{c} \sum_{j=1}^N \sum_{k \notin \mathcal{G}_3} C_{ij}^k x_j(t) x_k(t) - \frac{1}{c} \sum_{j=1}^N \sum_{k \notin \mathcal{G}_3} C_{ji}^k x_i(t) x_k(t) \\ & + d_i (g_i - x_i(t)) - \mu(t) x_i(t). \end{aligned} \quad (1)$$

The first and the second terms represent the catalytic reactions incoming to and outgoing from the i -th chemical species, respectively. The tensor $\{C_{ij}^k\}$ encodes the topology of catalytic reaction network, where C_{ij}^k is equal to 1 if reaction $j + k \rightarrow i + k$ exists, and is equal to 0 otherwise. c is the mean connectivity of the network, i.e., $\frac{1}{N} \sum_{i,j,k} C_{ij}^k = c$. The third and fourth terms represent the interaction with the external environment and dilution due to cell growth, respectively. By taking the sum of Eq. (1) over i , one finds $\sum_{i=1}^N \dot{x}_i(t) = \mu(t)(N - \sum_{i=1}^N x_i(t))$; hence, positive $\mu(t)$ enforces a constraint on the long-time behavior of the average abundance of chemical species, leading to

$$\lim_{t \rightarrow \infty} \frac{1}{N} \sum_{i=1}^N x_i(t) = 1. \quad (2)$$

If $\mu < 0$, the cell shrinks and eventually dies. In the model, we assume constant catalytic reaction rates following previous studies [41, 47]. We do not explicitly account for cell division, as its inclusion does not affect the conclusions of the analysis presented below.

To derive the effective dynamical equations on random networks, we adopt the configuration model [32, 57, 61, 62], which allows the construction of random networks with arbitrary distributions of in-degrees $p_u^{(\text{in})}$ and out-degrees $p_v^{(\text{out})}$, both having mean c , and catalytic degrees $p_w^{(\text{cat})}$ with mean $c/(\alpha_1 + \alpha_2)$. To construct a network, we first independently draw the degrees u_i, v_i , and w_i for each node from distributions $p_u^{(\text{in})}, p_v^{(\text{out})}$, and $p_w^{(\text{cat})}$, respectively. For nodes belonging to \mathcal{G}_3 , we set $w_i = 0$ because nutrients are catalytically inactive. The connection C_{ij}^k is then set to 1 with probability $u_i v_j w_k / (Nc)^2$ and to 0 otherwise. For sufficiently large N , this construction yields networks with the prescribed degree distributions. Below, we consider three kinds of distributions: a Poisson distribution (corresponding to the ER network), a uniform distribution defined on the interval $[(1-r)c, (1+r)c]$ ($0 < r \leq 1$), and a power-law distribution with exponent β ($2 < \beta$), which are displayed in Figs 1(b), (c) and (d), respectively. Networks with uniform or power-law degree distributions retain structural heterogeneity even in the dense limit, $c \rightarrow \infty$, whereas the ER network approaches a regular (homogeneous) random network.

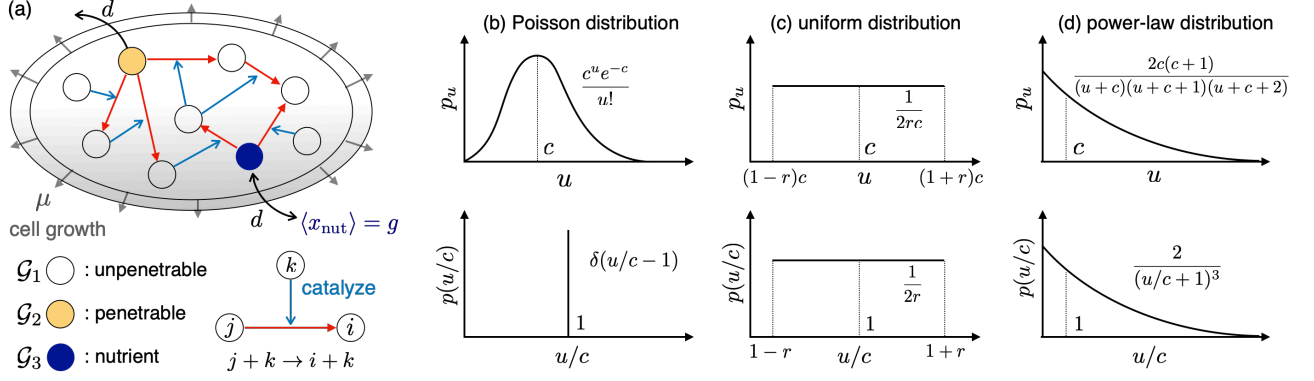


FIG. 1. (a) Schematic illustration of a model of a cell incorporating catalytic reactions, nutrient uptake, and cell growth. The catalytic reaction $j + k \rightarrow i + k$ represents the conversion of the chemical species j into the i catalyzed by the k . The model consists of three groups of chemical species: unpenetrable metabolic products, penetrable metabolic products, and nutrients, denoted by \mathcal{G}_1 , \mathcal{G}_2 and \mathcal{G}_3 , respectively. Nutrients are catalytically inactive. Penetrable metabolic products and nutrients can pass through the cell membrane with the permeability d . Their equilibrium abundances in the external environment are 0 and g , respectively. The cell grows at a rate μ , which is also a dynamical variable. Schematic illustrations of (b) Poisson, (c) uniform, and (d) power-law ($\beta = 3$) distributions with average connectivity c . Distributions of sparse and dense regimes are displayed at the top and bottom, respectively.

III. RESULTS

A. Effective dynamical equations and fixed points

In the thermodynamic limit, $N \rightarrow \infty$, and dense connectivity, $c \gg 1$, we analyze the dynamics governed by Eq. (1) using DMFT. By averaging over the network topology for given degree distributions, the effective dynamical equations for the typical abundances of chemical species belonging to \mathcal{G}_n with in-degree u and out-degree v are obtained exactly. The resulting dynamics is independent of the catalytic degree w because the catalyzed chemical species do not provide feedback through the catalytic activity. The derivation of the DMFT equations is presented in the Supplemental Material. The effective dynamical equations are given by

$$\dot{x}_{nuv}(t) = \frac{u}{c} m_{\text{in}}(t) m_{\text{cat}}(t) - \frac{v}{c} m_{\text{cat}}(t) x_{nuv}(t) + d_n (g_n - x_{nuv}(t)) - \mu(t) x_{nuv}(t), \quad (3)$$

where $m_{\text{in}}(t) = \sum_{n,u,v} \frac{v}{c} \alpha_n p_u^{(\text{in})} p_v^{(\text{out})} x_{nuv}(t)$ and $m_{\text{cat}}(t) = (\alpha_1 m_1(t) + \alpha_2 m_2(t)) / (\alpha_1 + \alpha_2)$. $m_n(t) = \sum_{u,v} p_u^{(\text{in})} p_v^{(\text{out})} x_{nuv}(t)$ represents the average abundance of chemical species belonging to \mathcal{G}_n . Hence, m_{cat} is regarded as the average abundance of catalytic chemical species. The growth rate is given by $\mu(t) = d(\alpha_3 g - \alpha_2 m_2(t) - \alpha_3 m_3(t))$. By taking the average of Eq. (3) over u, v , and n , and using the definition of $m_{\text{in}}(t)$, one finds that the average abundance of all chemical species converges to

$$\lim_{t \rightarrow \infty} (\alpha_1 m_1(t) + \alpha_2 m_2(t) + \alpha_3 m_3(t)) = 1 \quad (4)$$

if $\mu(t) > 0$, corresponding to Eq. (2).

At the fixed point, the following relation holds:

$$x_{nuv}^* = \frac{d_n g_n + \frac{u}{c} m_{\text{in}}^* m_{\text{cat}}^*}{d_n + \mu^* + \frac{v}{c} m_{\text{cat}}^*}, \quad (5)$$

where $A^* = \lim_{t \rightarrow \infty} A(t)$. One finds that the chemical abundance increases with increasing in-degree u and decreases with increasing out-degree v . By averaging x_{nuv}^* over u and v , we obtain

$$m_n^* = (d_n g_n + m_{\text{in}}^* m_{\text{cat}}^*) X(\mu^* + d_n, m_{\text{cat}}^*), \quad (6)$$

where $X(a, b) = \sum_v p_v^{(\text{out})} / (a + \frac{v}{c} b)$. Notably, m_n^* does not depend on the in-degree distribution; hence, macroscopic quantities such as μ^* and m_{cat}^* are independent of the in-degree distribution. Using the definitions of μ^* and m_{cat}^* , together with Eq. (4), we obtain a closed set of equations for μ^* , m_{in}^* , and m_{cat}^* :

$$m_{\text{in}}^* m_{\text{cat}}^* = \frac{(\alpha_1 + \alpha_2) m_{\text{cat}}^*}{\alpha_1 X(\mu^*, m_{\text{cat}}^*) + \alpha_2 X(\mu^* + d, m_{\text{cat}}^*)}, \quad (7)$$

$$m_{\text{in}}^* m_{\text{cat}}^* = \frac{d \alpha_3 g (1 - d X(\mu^* + d, m_{\text{cat}}^*)) - \mu^*}{d (1 - \alpha_1) X(\mu^* + d, m_{\text{cat}}^*)}, \quad (8)$$

$$m_{\text{in}}^* m_{\text{cat}}^* = \frac{1 - d \alpha_3 g X(\mu^* + d, m_{\text{cat}}^*)}{\alpha_1 X(\mu^*, m_{\text{cat}}^*) + (1 - \alpha_1) X(\mu^* + d, m_{\text{cat}}^*)}. \quad (9)$$

These equations admit two distinct solutions, corresponding to an overnutrition state and a metabolic state. In the overnutrition state, the cell is occupied solely by nutrients, i.e., $m_{\text{cat}}^* = 0$, immediately obtained from Eq. (7). Since nutrients are catalytically inactive, no catalytic reactions occur inside the cell in this state. Accordingly, x_{1uv}^* and x_{2uv}^* vanish, while $x_{3uv}^* = 1/\alpha_3$ for any u and v . The growth rate is then given by $\mu^* = d(\alpha_3 g - 1)$,

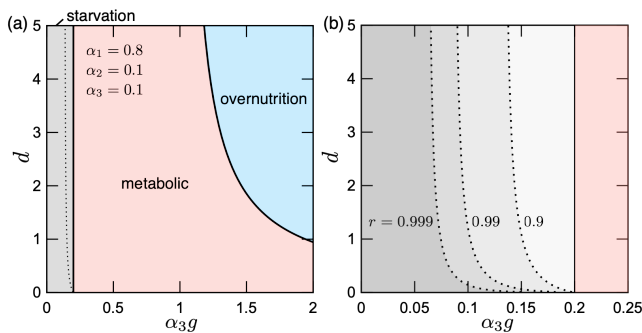


FIG. 2. (a) Phase diagram in the dense-network limit for the parameters $(\alpha_1, \alpha_2, \alpha_3) = (0.8, 0.1, 0.1)$. The solid curve represents the boundary d_c between metabolic and overnutrition states, given in Eq. (10). The solid vertical line, $\alpha_3 g = 1 - \alpha_1$, and dashed curve represent the boundary between metabolic and starvation states for Poisson and uniform ($r = 0.9$) distributions, respectively. (b) Phase diagram for low $\alpha_3 g$ with $(\alpha_1, \alpha_2, \alpha_3) = (0.8, 0.1, 0.1)$. The phase boundaries between the metabolic and starvation states for $r = 0.9, 0.99$, and 0.999 are shown.

which is independent of both the in- and out-degree distributions. By contrast, in the metabolic state, all chemical species have finite abundances, and catalytic reactions are sustained within the cell. For Poisson and uniform degree distributions, the cell growth rates of both solutions become negative if the nutrient supply is too small. Then, the convergence condition of Eq. (4) is violated, indicating that the cell shrinks and eventually dies. In this study, we define the state located in this parameter region as a starvation state.

B. Phase diagram

We first present in Fig. 2(a) the phase diagram in the $(\alpha_3 g, d)$ plane for $(\alpha_1, \alpha_2, \alpha_3) = (0.8, 0.1, 0.1)$. For large $\alpha_3 g$, the transition between metabolic and overnutrition states occurs. The phase boundary is given by

$$d_c = \frac{\alpha_3 g - \alpha_2 / (\alpha_1 + \alpha_2)}{\alpha_3 g (\alpha_3 g - 1)}, \quad (10)$$

which is obtained from a linear stability analysis of the overnutrition solution [55, 63] (see Appendix B for the derivation). Notably, the onset of instability is independent of the degree distribution. The system tends to be in an overnutrition state at higher values of $\alpha_3 g$ and d , where nutrient supply dominates and effectively suppresses catalytic reactions. Moreover, the phase boundary shifts downward with an increasing fraction of penetrable metabolic products α_2 , since they are subject to a loss of abundance through interaction with the external environment.

In contrast to the metabolic-overnutrition transition, the boundary of the metabolic-starvation transition at low $\alpha_3 g$ depends sensitively on the out-degree distribu-

tions, as shown in Fig. 2(b). For the Poisson distribution, the boundary is $\alpha_3 g = 1 - \alpha_1$ at which the cell growth rate becomes negative (see Appendix C), whereas for uniform and power-law distributions, the metabolic state persists even for $\alpha_3 g < 1 - \alpha_1$. In particular, the starvation phase disappears for the power-law distribution. For the uniform distribution, the phase boundary shifts downward with increasing the heterogeneity parameter r , and the starvation phase disappears at $r = 1$. Notice that even for values very close to $r = 1$, such as $r = 0.999$, the phase boundary remains robustly present, indicating $r = 1$ is singular. We will present the behaviors of physical quantities at low $\alpha_3 g$ and the reason for the disappearance of the starvation state in detail in Sec. III D.

C. Transition between metabolic and overnutrition states

We now present the behavior of the physical quantities in the metabolic-overnutrition transition that occurs at high nutrient supply. Since the metabolic solution depends on the out-degree distribution, we analyze it for Poisson, uniform, and power-law distributions, which yield homogeneous, moderately heterogeneous, and strongly heterogeneous networks in the dense limit, respectively. For the Poisson degree distribution, the metabolic solution can be derived analytically (see Appendix C for details). By contrast, for the uniform and power-law degree distributions, the solution is not available analytically and is therefore obtained numerically using the Levenberg-Marquardt algorithm [64].

Figures 3(a) and (b) show the growth rate μ^* and the average abundance of the catalytic chemical species m_{cat}^* , respectively, as functions of d , for $\alpha_3 g = 1.5$, $\alpha_1 = 0.8$, and $\alpha_2 = 0.1$. The value of μ^* for $d < d_c$ is largest in the Poisson case and smallest in the power-law case, suggesting that increasing network heterogeneity suppresses the growth rate for high $\alpha_3 g$. As d approaches d_c , μ^* converges to the same value, and the system undergoes a transition to the non-metabolic state via a transcritical bifurcation at $d = d_c$. Likewise, m_{cat}^* decays to zero continuously, as shown in Fig. 3(b).

To examine the range of validity of our theory with respect to network connectivity, c , we perform numerical simulations of Eq. (1) on ER and dBA networks with finite connectivity and $N = 1.0 \times 10^5$ (see Appendix A for details). Here, the dBA networks have the power-law out-degree distribution with exponent $\beta = 3$ and homogeneous in-degrees. In Figs. 3(c) and (d), we show $\mu(t)$ and $m_{\text{cat}}(t)$ evaluated at $t = 100$, which is sufficiently long for the system to reach the fixed point, except in the vicinity of the transition point for small connectivities (see Figs. 6(a) and (b) in Appendix A). The data for $c = 50, 20, 10$ collapse onto the DMFT result, indicating that the network with $c \gtrsim 10$ is sufficiently dense. For $c < 10$, the data agree with the DMFT result at small d but exhibit a sudden shift to the overnutrition

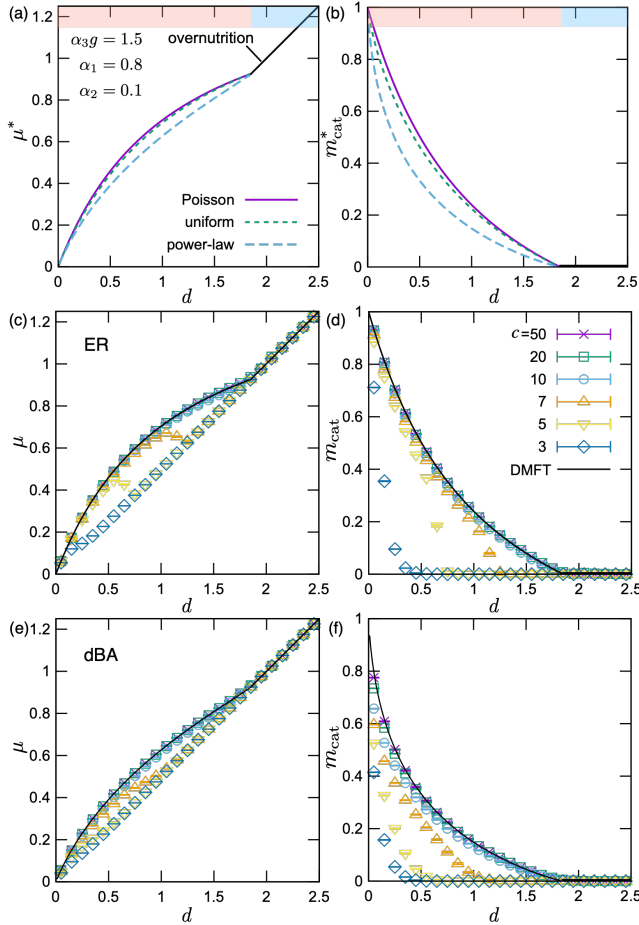


FIG. 3. Dependence on permeability d of (a) the growth rate μ^* and (b) the average abundance of catalytic chemical species m_{cat}^* in steady state, obtained from the DMFT. In the metabolic state $d < d_c \approx 1.85$, different colors represent different network topologies: results for Poisson, uniform ($r = 1$), and power-law degree distributions (exponent $\beta = 3$) are shown from top to bottom. The black line for $d > d_c$ represents the non-metabolic state. Dependence on d of (c) $\mu(t)$ and (d) $m_{\text{cat}}(t)$ at $t = 100$ for the ER networks with system size $N = 10^5$ and finite connectivities $c = 50, 20, 10, 7, 5$, and 3. Dependence on d of (e) $\mu(t)$ and (f) $m_{\text{cat}}(t)$ at $t = 100$ for the dBA networks with system size $N = 10^5$ and finite connectivities $c = 50, 20, 10, 7, 5$, and 3. The dense-limit result from the DMFT is also shown for comparison. $\alpha_3 g = 1.5$, $\alpha_1 = 0.8$, and $\alpha_2 = 0.1$ are used in all panels. The simulation data are averaged over 100 network realizations.

state below the DMFT transition point. Thus, network sparseness destabilizes the metabolic state. Similar to ER networks, the data for $c = 50, 20, 10$ on the dBA networks exhibit a good agreement with the DMFT result for the power-law distribution, as shown in Figs. 3(e) and (f). For $c < 10$, μ gradually shifts downward from the DMFT result with increasing d . This is also due to the destabilization of the metabolic state.

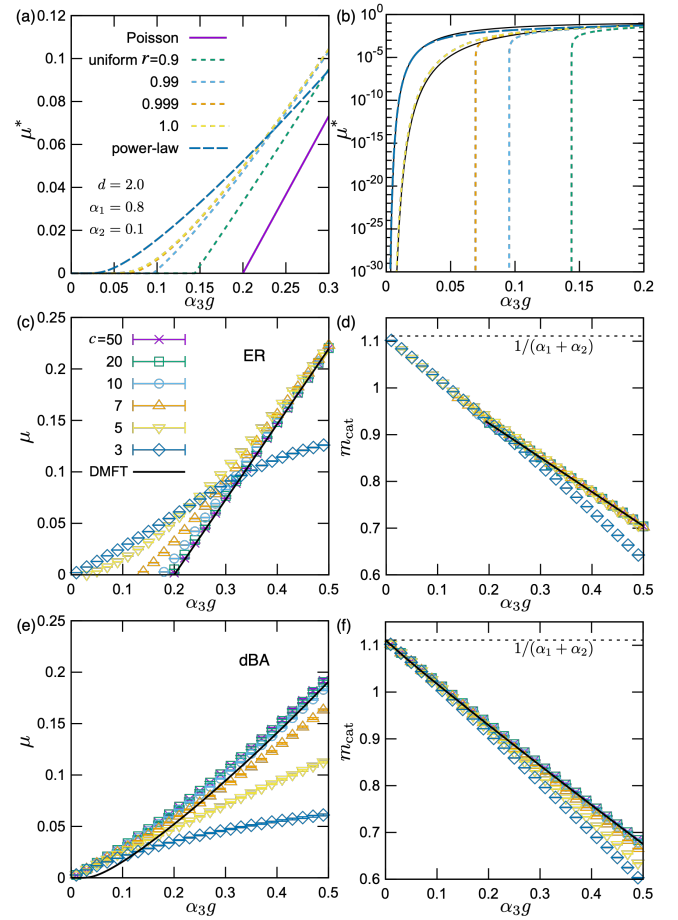


FIG. 4. (a) Dependence on nutrient supply $\alpha_3 g$ of the growth rate μ^* obtained from the DMFT and (b) its semi-log plot. Different colors represent different network topologies: results for Poisson, uniform ($r = 0.9, 0.99, 0.999, 1$), and power-law degree distributions (exponent $\beta = 3$) are shown. The black solid curves in panel (b) represent asymptotic solutions for $\alpha_3 g \ll 1$. Dependence on $\alpha_3 g$ of (c) $\mu(t)$ and (d) $m_{\text{cat}}(t)$ at $t = 100$ for the ER networks with system size $N = 10^5$ and finite connectivities $c = 50, 20, 10, 7, 5$, and 3. Dependence on $\alpha_3 g$ of (e) $\mu(t)$ and (f) $m_{\text{cat}}(t)$ at $t = 100$ for the dBA networks with system size $N = 10^5$ and finite connectivities $c = 50, 20, 10, 7, 5$, and 3. The dense-limit result from the DMFT is also shown for comparison. The dotted horizontal lines in panels (d) and (f) represent the maximum value of m_{cat} , $1/(\alpha_1 + \alpha_2)$. $d = 2.0$, $\alpha_1 = 0.8$, and $\alpha_2 = 0.1$ are used in all panels. The simulation data are averaged over 100 network realizations.

D. Transition between metabolic and starvation states

Next, we present the DMFT results for low nutrient supply. Figure 4(a) displays the $\alpha_3 g$ dependence of the growth rate μ^* for Poisson, uniform ($r = 0.9, 0.99, 0.999, 1$), and power-law ($\beta = 3$) out-degree distributions with $d = 2.0$, $\alpha_1 = 0.8$, and $\alpha_2 = 0.1$. One finds that the value of μ^* is smallest in the Poisson case and largest in the power-law case for low $\alpha_3 g$, suggest-

ing that a more heterogeneous network yields a higher growth rate, in contrast to the behavior at high $\alpha_3 g$. Indeed, for the uniform distribution, μ^* increases as the heterogeneity parameter r increases. Furthermore, network heterogeneity makes cells more resilient to nutrient starvation. While μ^* becomes zero and exhibits a metabolic-starvation transition at $\alpha_3 g = 1 - \alpha_1$ for the Poisson distribution (see also Appendix C), the transition point shifts to lower $\alpha_3 g$ values for the uniform distribution with larger r , and disappears only when $r = 1$, as shown in Fig. 4(b). The power-law distribution also does not exhibit such a transition. Mathematically, these disappearances of the metabolic-starvation transitions originate from the fact that $X(\mu^*, m_{\text{cat}}^*)$ appearing in m_1^* , given by Eq. (6), exhibits a logarithmic divergence as $\mu^* \rightarrow +0$ (see Appendix D in detail). This divergence makes the mean abundance of unpenetrable metabolic products m_1^* , significantly larger than those of the other species, m_2^* and m_3^* . More specifically, the logarithmic divergence of $X(\mu^*, m_{\text{cat}}^*)$ stems from the divergence of x_{1uv}^* , given by Eq. (5), in the $v/c \rightarrow 0$. This means that the existence of the starvation state depends on whether the network contains unpenetrable metabolic products with extremely small out-degrees, such that their outgoing reactions are negligible relative to their incoming reactions. The asymptotic behavior of μ^* at $\alpha_3 g \ll 1$ can be shown to take the exponential form $\mu^* \sim \exp(-C/\alpha_3 g)$, for both the uniform distribution with $r = 1$ and the power-law distribution with $\beta = 3$, where C is a positive constant (see Eq. (D6) in Appendix D and Fig. 4(b)). Therefore, the cell growth rate μ^* becomes close to zero but remains positive for any $\alpha_3 g > 0$.

In the same manner as in the high $\alpha_3 g$ case, we also test the validity of the DMFT results with respect to network connectivity c by performing numerical simulations of Eq. (1) for low $\alpha_3 g$ on ER and dBA networks with finite connectivity and $N = 1.0 \times 10^5$. In Figs. 4 (c) and (d), we show $\mu(t)$ and $m_{\text{cat}}(t)$ evaluated at $t = 100$. $\mu(t)$ for $c = 50$ agrees well with the DMFT result but deviates upward for $c \leq 20$. The transition point shifts to lower $\alpha_3 g$ as c decreases, and disappears for $c = 3$, indicating that the network sparseness helps to avoid starvation. On the other hand, $\mu(t)$ for $c = 3$ becomes significantly smaller than the other data when $\alpha_3 g > 0.3$. In fact, in this parameter region, the dynamics have not yet converged at $t = 100$ and appear to relax toward the overnutrition state (see Figs. 6(c) and (d) in Appendix A). Thus, while sparseness stabilizes metabolism at low $\alpha_3 g$, under nutrient-rich conditions the metabolic state becomes unstable, which is consistent with Fig. 3(c). m_{cat} for all c except $c = 3$ collapses well onto the DMFT result, but extends into the region $\alpha_3 g < 1 - \alpha_1$. As $\alpha_3 g$ decreases, m_{cat} approaches its maximum value, $1/(\alpha_1 + \alpha_2)$, which corresponds to the limit $m_3 = 0$. Simulation results for low $\alpha_3 g$ on the dBA networks do not show perfect agreement with the DMFT results, even when c is large. As shown in Figs. 4(e) and (f), $\mu(t)$ for $c = 50, 20$ is

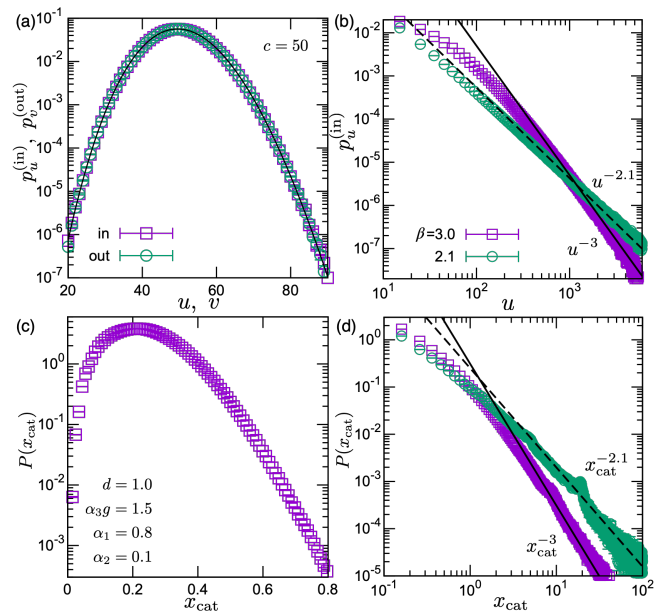


FIG. 5. Semi-log plots of the distribution of (a) the in- and out-degree distributions, $p_u^{(\text{in})}$, $p_v^{(\text{out})}$, and (c) the abundance distribution of catalytic chemical species, $P(x_{\text{cat}})$, for the ER network. The black curve in (a) represents the Poisson distribution. Log-log plots of (b) the in-degree distribution $p_u^{(\text{in})}$ and (d) the abundance distribution of catalytic chemical species, $P(x_{\text{cat}})$, for the dBA network with power-law in-degree distributions with the exponents $\beta = 3.0$ and 2.1 . Simulations are performed with parameters $N = 5.0 \times 10^5$, $c = 50$, $d = 1.0$, $\alpha_3 g = 1.5$, $\alpha_1 = 0.8$ and $\alpha_2 = 0.1$ and averaged over 100 network realizations.

slightly higher than the DMFT result, while $m_{\text{cat}}(t)$ collapses onto the DMFT result. This discrepancy may be attributed to the small degree correlation between connected nodes in the dBA network [65], which is not accounted for in our DMFT. Nevertheless, even with such an effect, the transition to the starvation state does not occur in scale-free networks.

E. Distributions in abundances of biomolecules

We now turn to the distributions of chemical abundances. In particular, to understand the power-law behavior observed experimentally in biomolecules [41–45], we consider the abundance distributions of chemical species belonging to \mathcal{G}_1 and \mathcal{G}_2 ; that is, the abundance distributions of catalytic chemical species. One readily finds from Eq. (5) that the typical abundance of these species is proportional to their in-degree; hence, when the in-degree distribution follows a power law, the abundance distribution also follows a power law with a common exponent. To confirm this theoretical prediction, we numerically sample the abundance distributions of catalytic chemical species $P(x_{\text{cat}})$ on the ER and dBA networks with in-degree power-law distributions.

The degree distributions of ER and dBA networks are shown in Figs. 5 (a) and (b). The in- and out-degree distributions of the ER network follow Poisson distributions. On the other hand, the in-degree distribution of the dBA network follows a power law $u^{-\beta}$, whose exponent can be controlled within the range $\beta > 2$ [11, 60] (see Appendix A in detail). For the ER network, the abundance distribution does not have a fat tail, as shown in Fig. 5 (c). This behavior reflects the in-degree Poisson distribution and is clearly distinguished from a power law. In contrast, for the dBA network, power-law tails are observed in the abundance distributions, with exponents identical to those of the in-degree distribution, as shown in Fig. 5 (d). This agreement confirms the theoretical prediction that the abundance statistics of metabolic products directly reflect the underlying network topology.

IV. DISCUSSION AND SUMMARY

In summary, we exactly solve a dense simple catalytic reaction network model with arbitrary degree distributions using DMFT. We show that the boundary of the metabolic-starvation transition sensitively depends on the out-degree distribution, whereas the boundary of the metabolic-overnutrition transition does not. In particular, a power-law distribution of out-degrees suppresses the transition to the starvation state. Although heterogeneous out-degree distribution is disadvantageous for cellular growth under nutrient-rich conditions, it becomes advantageous under nutrient-poor conditions, preventing the system from entering the starvation state. To test the validity of the DMFT results, we also performed numerical simulations on networks with finite connectivity, c . Under nutrient-rich conditions, the DMFT results agree well with simulations down to $c \approx 10$, whereas for $c < 10$ the metabolic state becomes unstable and transitions to the overnutrition state. In contrast, under nutrient-poor conditions, network sparseness further stabilizes the metabolic state. We further found that the abundance of metabolic products is proportional to the node's in-degree. Consequently, the abundance of metabolic products exhibits a power-law tail when the in-degree distribution also has a power-law structure with a common exponent, which is confirmed by numerical simulations on the dBA network.

In real cells, gene expression levels are often presented as a rank-ordered distribution, with the exponent β' typically between 0.9 and 1.0 [41–45]. The exponent β of the original abundance distribution is related to β' via the relation $\beta = (\beta' + 1)/\beta'$. Using this relation yields $\beta \approx 2.1$, which is remarkably close to the experimentally observed exponent of approximately 2.2 for the degree distribution of metabolic networks [12].

The mechanism underlying the disappearance of the metabolic-starvation transition on scale-free networks differs from those known in other systems, such as the Ising models [35] and epidemic spreading models [36]. In

those systems, the absence of a transition is typically attributed to highly connected hub nodes with large degrees. By contrast, in the present model, the transition disappears due to the presence of many nodes with extremely small out-degrees. In particular, unpenetrable metabolic products with small out-degrees relative to their in-degrees retain catalytic activity within the cell, preventing the system from losing mass and avoiding cellular shrinkage. This interpretation is consistent with the fact that the starvation transition is absent even for the uniform distribution with $r = 1$, which does not possess a heavy tail.

It is worth noting that real metabolic networks are more complex than the present model, and that their scale-free network structure arises through evolution [12, 47]. We consider the network average for typical realizations with power-law degree distributions, although networks generated by evolution are not typical but rather finely tuned and exceptional structures [66, 67]. For instance, hub chemical species and the species connected to them are not chosen at random [12]. Moreover, we do not take into account correlations between connecting nodes (clustering property) and among in-degree, out-degree, and catalytic degree, which may change the dynamical behaviors. Even in the dBA networks, which have small degree correlations between nodes [65], we observed a slight deviation from the DMFT results (see Fig. 4(e)). Nevertheless, we provide an exact analytical description for typical realizations with power-law degree distributions. Our results, therefore, provide a valuable baseline for comparison with dynamics on more realistic networks, including those generated by evolutionary processes.

ACKNOWLEDGMENTS

The authors would like to thank Kunihiro Kaneko, Chikara Furusawa, Yoshiyuki Kabashima, Hajime Yoshino, Toshinori Namba, and Dominic K. Devlin for valuable discussions. This work was supported by JSPS KAKENHI Grant No. 25K17354, 24K00594, and No. 24H01931 from MEXT, Japan.

Appendix A: Setups and dynamical behaviors of numerical simulations

Construction of sparse networks

We specify the catalytic reaction network by a binary adjacency tensor $C_{ij}^k \in \{0, 1\}$. The tensor C_{ij}^k is equal to 1 if the reaction $j + k \rightarrow i + k$ exists, and is equal to 0 otherwise. The catalytic reaction network is generated in three steps. We first construct a directed network described by an adjacency matrix $A_{ij} \in \{0, 1\}$, where $A_{ij} = 1$ means that the reaction channel $j \rightarrow i$ is allowed. Next, we assign to each node i one of the following groups: unpenetrable metabolic product ($n = 1$), penetrable metabolic product ($n = 2$), or nutrient ($n = 3$).

The fractions of these species are fixed to be α_1 , α_2 , and α_3 , respectively, with $\alpha_1 + \alpha_2 + \alpha_3 = 1$. Finally, for each directed edge $A_{ij} = 1$, we independently assign a catalyst species k chosen uniformly at random from the set of non-nutrient species ($n = 1, 2$) [41]. In the case of Erdős-Rényi (ER) random networks, A_{ij} is set to 1 with probability c/N and to 0 otherwise [11, 32, 59]. In the case of directed Barabási-Albert (dBA) networks, A_{ij} is generated via evolution with preferential attachment rule [11, 60]. The preferential attachment rule to generate dBA network with a power-law in-degree distribution is as follows:

1. Prepare a complete directed network (without self-loops) consisting of $c + 1$ nodes as the initial state.
2. Add one new node to the network.
3. Create c outgoing edges from the newly added node to existing nodes. Each endpoint node i is chosen independently with probability $(u_i + A/c) / \sum_{i'} (u_{i'} + A/c)$, where u_i denotes the current value of the in-degree of node i , and A is the homogeneous attractiveness parameter. When selecting endpoints for the c outgoing edges, we reject duplicates so that the new node connects to c distinct existing nodes.
4. Repeat steps 2–3 until the total number of nodes reaches N .

With the above preferential-attachment rule, the resulting stationary in-degree distribution has a power-law tail, $p_u^{(\text{in})} \sim u^{-\beta}$ with $\beta = 2 + A/c$. Thus, the attractiveness parameter A continuously tunes the tail exponent. Since each newly added node creates exactly c outgoing edges, its out-degree distribution becomes $p_v^{(\text{out})} = \delta_{v,c}$. If the roles of in-degree and out-degree is reversed, we can also generate dBA network with a power-law out-degree distribution.

Dynamics

For the simulation under high nutrient supply ($\alpha_3 g > 1$), we set $x_i = 1$ for all i as the initial condition. On the other hand, for the simulation under low nutrient supply ($\alpha_3 g < 1$), we set $x_i = (2 - \alpha_3 g)/2\alpha_1$ for $i \in \mathcal{G}_1$ and $x_i = \alpha_3 g/2(\alpha_2 + \alpha_3)$ for $i \in \mathcal{G}_2, \mathcal{G}_3$ as the initial condition to avoid a negative growth rate at $t = 0$. Then, the initial value of μ becomes $\alpha_3 g d/2$. We solve Eq. (1) by using the fourth-order Runge-Kutta method. The time resolution $\Delta t = 0.02$ is used. We display the dynamical behaviors of the cellular growth rate $\mu(t)$ for various situations in Fig. 6. One finds that $t = 100$ is sufficient to reach the fixed point for networks with $c \geq 10$.

Appendix B: Linear stability analysis

To examine the stability of the non-metabolic solution, we linearize the DMFT equation (Eq. (3)) around the fixed point by introducing a small perturbation

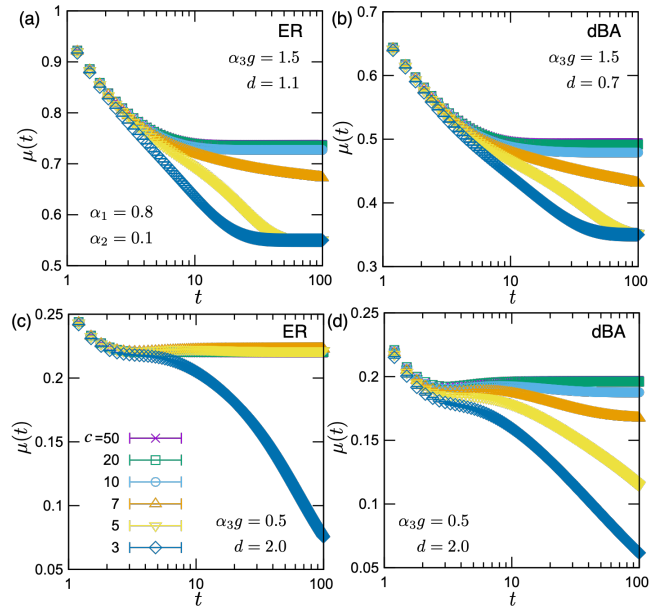


FIG. 6. Time dependence of growth rate $\mu(t)$ at (a) $(\alpha_3 g, d) = (1.5, 1.1)$ and (c) $(\alpha_3 g, d) = (0.5, 2.0)$ for ER networks and (b) $(\alpha_3 g, d) = (1.5, 0.7)$ and (d) $(\alpha_3 g, d) = (0.5, 2.0)$ for dBA networks with finite connectivity $c = 50, 20, 10, 7, 5$ and 3 . Simulations are performed with parameters $N = 1.0 \times 10^5$, $\alpha_1 = 0.8$ and $\alpha_2 = 0.1$ and averaged over 100 network realizations.

$\xi_{nuv}(t)$ [55, 63]. The perturbation is assumed to be an independent white Gaussian noise for each n , u , and v . We define the deviations from the fixed point as $\delta x_{nuv}(t) = x_{nuv}(t) - x_{nuv}^*$, $\delta m_{\text{cat}}(t) = m_{\text{cat}}(t) - m_{\text{cat}}^*$, $\delta m_{\text{in}}(t) = m_{\text{in}}(t) - m_{\text{in}}^*$, and $\delta \mu(t) = \mu(t) - \mu^*$. If the solution is stable, all these deviations fluctuate around zero in the long-time limit.

The linearized dynamics around a given fixed point are written as

$$\begin{aligned} \delta \dot{x}_{nuv}(t) = & \frac{u}{c} (m_{\text{in}}^* \delta m_{\text{cat}}(t) + \delta m_{\text{in}}(t) m_{\text{cat}}^*) \\ & - \frac{v}{c} (m_{\text{cat}}^* \delta x_{nuv}(t) + \delta m_{\text{cat}}(t) x_{nuv}^*) \\ & - (d_n + \mu^*) \delta x_{nuv}(t) - \delta \mu(t) x_{nuv}^* + \xi_{nuv}. \end{aligned} \quad (\text{B1})$$

Denoting by $\tilde{f}(\omega)$ the Fourier transform of a function $f(t)$, Eq. (B1) can be rewritten as

$$\begin{aligned} \delta \tilde{x}_{nuv}(\omega) = & \frac{\frac{u}{c} (m_{\text{in}}^* \delta \tilde{m}_{\text{cat}}(\omega) + \delta \tilde{m}_{\text{in}}(\omega) m_{\text{cat}}^*)}{i\omega + d_n + \mu^* + \frac{v}{c} m_{\text{cat}}^*}}{\frac{\frac{v}{c} \delta \tilde{m}_{\text{cat}}(\omega) - \delta \tilde{\mu}(\omega) x_{nuv}^* + \tilde{\xi}_{nuv}(\omega)}{i\omega + d_n + \mu^* + \frac{v}{c} m_{\text{cat}}^*}}}. \end{aligned} \quad (\text{B2})$$

Substituting the non-metabolic solution into Eq. (B2),

we obtain the following expressions for

$$\delta\tilde{x}_{1uv}(\omega) = \frac{\frac{u}{c}\delta\tilde{m}_{\text{cat}}(\omega) + \tilde{\xi}_{1uv}(\omega)}{i\omega + d(\alpha_3g - 1)}, \quad (\text{B3})$$

$$\delta\tilde{x}_{2uv}(\omega) = \frac{\frac{u}{c}\delta\tilde{m}_{\text{cat}}(\omega) + \tilde{\xi}_{2uv}(\omega)}{i\omega + d\alpha_3g}, \quad (\text{B4})$$

$$\delta\tilde{x}_{3uv}(\omega) = \frac{\frac{u-v/\alpha_3}{c}\delta\tilde{m}_{\text{cat}}(\omega) - \delta\tilde{\mu}(\omega)/\alpha_3 + \tilde{\xi}_{3uv}(\omega)}{i\omega + d\alpha_3g}. \quad (\text{B5})$$

We then square these expressions and average over the Gaussian noise ξ_{nuv} to obtain

$$\langle |\delta\tilde{x}_{1uv}(\omega)|^2 \rangle = \frac{(\frac{u}{c})^2 \langle |\delta\tilde{m}_{\text{cat}}(\omega)|^2 \rangle + I_{1uv}}{\omega^2 + d^2(\alpha_3g - 1)^2}, \quad (\text{B6})$$

$$\langle |\delta\tilde{x}_{2uv}(\omega)|^2 \rangle = \frac{(\frac{u}{c})^2 \langle |\delta\tilde{m}_{\text{cat}}(\omega)|^2 \rangle + I_{2uv}}{\omega^2 + d^2\alpha_3^2g^2}, \quad (\text{B7})$$

$$\langle |\delta\tilde{x}_{3uv}(\omega)|^2 \rangle = \frac{\langle \left| \frac{(u-v/\alpha_3)\delta\tilde{m}_{\text{cat}}}{c} - \frac{\delta\tilde{\mu}(\omega)}{\alpha_3} \right|^2 \rangle + I_{3uv}}{\omega^2 + d^2\alpha_3^2g^2}, \quad (\text{B8})$$

where $\langle \dots \rangle$ denotes the average over ξ_{nuv} and $I_{nuv} = \langle |\tilde{\xi}_{nuv}|^2 \rangle$. In the limit $\omega \rightarrow 0$, one finds that $\langle |\delta\tilde{x}_{1uv}(\omega)|^2 \rangle$ diverges at $\alpha_3g = 1$, whereas $\langle |\delta\tilde{x}_{2uv}(\omega)|^2 \rangle$ and $\langle |\delta\tilde{x}_{3uv}(\omega)|^2 \rangle$ diverge at $\alpha_3g = 0$. Hence, for any permeability d , the non-metabolic state becomes unstable at $\alpha_3g = 1$ if $\alpha_1 > 0$, and otherwise at $\alpha_3g = 0$.

The non-metabolic state can be unstable even for $\alpha_3g > 1$ if the numerators in Eqs. (B6-B8) diverge. From the definition of the average catalytic abundance m_{cat} , we obtain the following self-consistent relation for

$$\delta\tilde{m}_{\text{cat}}(\omega) = \frac{1}{\alpha_1 + \alpha_2} \left(\alpha_1 \frac{\delta\tilde{m}_{\text{cat}}(\omega) + \tilde{\xi}_1(\omega)}{i\omega + d(\alpha_3g - 1)} + \alpha_2 \frac{\delta\tilde{m}_{\text{cat}}(\omega) + \tilde{\xi}_2(\omega)}{i\omega + d\alpha_3g} \right), \quad (\text{B9})$$

where $\tilde{\xi}_n = \sum_{u,v} p_u^{(\text{in})} p_v^{(\text{out})} \tilde{\xi}_{nuv}(\omega)$. Evaluating the zero-frequency limit of $\langle |\delta\tilde{m}_{\text{cat}}(\omega)|^2 \rangle$, we find

$$\langle |\delta\tilde{m}_{\text{cat}}(0)|^2 \rangle \propto \frac{1}{d^2 [d(\alpha_3g - 1)\alpha_3g - \frac{\alpha_1\alpha_3g + \alpha_2(\alpha_3g - 1)}{\alpha_1 + \alpha_2}]^2}. \quad (\text{B10})$$

The divergence of this quantity determines the critical permeability, d_c , given in Eq. (10). Hence, for $d < d_c$, the fluctuations $\langle |\delta\tilde{x}_{nuv}(\omega)|^2 \rangle$ diverge for all n, u , and v , leading to the instability of the non-metabolic solution, as shown in Fig. 2(a).

Appendix C: Metabolic solution for the Poisson degree distribution

In the dense connectivity limit, the Poisson out-degree distribution reduces to the Kronecker delta, $p_v^{(\text{out})} = \delta_{c,v}$.

As a result, $X(a, b) = \sum_v p_v^{(\text{out})} / (a + \frac{v}{c}b) = 1/(a+b)$ and $m_{\text{in}}^* = 1$. Substituting these relations into Eq. (7), we obtain

$$\alpha_1 + \alpha_2 = \frac{\alpha_1}{\mu^* + m_{\text{cat}}^*} + \frac{\alpha_2}{\mu^* + m_{\text{cat}}^* + d}. \quad (\text{C1})$$

Solving this equation yields

$$\begin{aligned} \mu^* + m_{\text{cat}}^* &= \frac{1 - d + \sqrt{(1-d)^2 + 4\alpha_1 d / (\alpha_1 + \alpha_2)}}{2} \\ &\equiv \phi(d, \alpha_1, \alpha_2). \end{aligned} \quad (\text{C2})$$

Here, we have used the fact that $\phi(d, \alpha_1, \alpha_2)$ must be positive. Substituting Eq. (C2) into Eqs. (7) and (8), we finally obtain the growth rate and the average catalytic abundance as

$$\mu^* = \frac{d(\alpha_3g + \alpha_1 - 1)\phi(d, \alpha_1, \alpha_2)}{\phi(d, \alpha_1, \alpha_2) + \alpha_1 d}, \quad (\text{C3})$$

$$m_{\text{cat}}^* = \frac{(\phi(d, \alpha_1, \alpha_2) - d(\alpha_3g - 1))\phi(d, \alpha_1, \alpha_2)}{\phi(d, \alpha_1, \alpha_2) + \alpha_1 d}, \quad (\text{C4})$$

which are shown in Figs. 3(a) and (b), respectively. Finally, substituting the critical point d_c , given by Eq. (10), into the above expressions, one can verify that the metabolic solution continuously connects with the over-nutrition solution, $\mu^* = d(\alpha_3g - 1)$ and $m_{\text{cat}}^* = 0$. In addition, one can easily find that μ^* becomes negative below $\alpha_3g < 1 - \alpha_1$, which indicates the transition to the starvation state.

Appendix D: Asymptotic solutions for low nutrient supply

In this section we consider the situation where $\mu^* \ll \alpha_3g \ll 1$ and $\mu^* \ll d$. We show that, for both the uniform distribution with $r = 1$ and the power-law distribution, the asymptotic behavior of μ^* as a function of α_3g exhibits the exponential form $\exp(-C/\alpha_3g)$, where C is a positive constant.

First, fixed-point values of the average abundances of unpenetrable metabolic products, penetrable metabolic products, and nutrients are given by

$$m_1^* = X(\mu^*, m_{\text{cat}}^*) m_{\text{in}}^* m_{\text{cat}}^*, \quad (\text{D1})$$

$$m_2^* \simeq X(d, m_{\text{cat}}^*) m_{\text{in}}^* m_{\text{cat}}^*, \quad (\text{D2})$$

$$m_3^* \simeq X(d, m_{\text{cat}}^*) (dg + m_{\text{in}}^* m_{\text{cat}}^*), \quad (\text{D3})$$

respectively, where we used Eq. (6). Substituting these into the definition of μ and using Eq. (4), we obtain the relation

$$X(\mu^*, m_{\text{cat}}^*) \simeq \frac{1 - \alpha_3g}{\alpha_1 m_{\text{in}}^* m_{\text{cat}}^*}. \quad (\text{D4})$$

Because the uniform distribution with $r = 1$ and the power-law distribution with $\beta = 3$ with dense connectivity, $c \gg 1$, are written as $p(v/c) = 1/2$ with the interval

$[0, 2]$ and $p(v/c) = 2/(1 + v/c)^3$ with the interval $[0, \infty)$, respectively, the function $X(a, b)$ can be evaluated as

$$\begin{aligned} X(a, b) &= \sum_v p_v^{(\text{out})} / (a + \frac{v}{c}) \\ &= \begin{cases} \int_0^2 dv' 1/2(a + v'b) & (\text{uniform}) \\ \int_0^\infty 2/(1 + v')^3(a + v'b) & (\text{power-law}) \end{cases} \\ &= \begin{cases} \frac{1}{2b} \log \frac{a+2b}{a} & (\text{uniform}) \\ \frac{1}{(a-b)^2} \left(\frac{2b^2}{a-b} \log \frac{b}{a} + a - 3b \right) & (\text{power-law}), \end{cases} \end{aligned} \quad (\text{D5})$$

where $v' = v/c$. One finds that the value of $X(a, b)$ logarithmically diverges as $a \rightarrow +0$. Thus, when $\mu^* \ll \alpha_3 g \ll 1$, the relation given by Eq. (D4) leads to

$$\mu^* = \begin{cases} 2m_{\text{cat}}^* \exp\left(-2\frac{1-\alpha_3 g}{\alpha_1 m_{\text{in}}^*}\right) & (\text{uniform}) \\ m_{\text{cat}}^* \exp\left(-\frac{3}{2} - \frac{1-\alpha_3 g}{2\alpha_1 m_{\text{in}}^*}\right) & (\text{power-law}). \end{cases} \quad (\text{D6})$$

Next, we derive m_{cat}^* and m_{in}^* as functions of $\alpha_3 g$. Using Eqs. (D4), (7), (D1), and (D2), we obtain

$$m_{\text{in}}^* = \frac{(\alpha_1 + \alpha_2)m_{\text{cat}}^* - 1 + \alpha_3 g}{m_{\text{cat}}^* \alpha_2 X(d, m_{\text{cat}}^*)}. \quad (\text{D7})$$

Using Eqs. (D1-D3) and (4), we obtain

$$m_{\text{in}}^* = \frac{(1 - dX(d, m_{\text{cat}}^*))\alpha_3 g}{(1 - \alpha_1)m_{\text{cat}}^* X(d, m_{\text{cat}}^*)}. \quad (\text{D8})$$

From Eqs. (D7) and (D8), we can derive the equation for m_{cat}^* as

$$(\alpha_1 + \alpha_2)m_{\text{cat}}^* - 1 + \alpha_3 g = \frac{\alpha_2(1 - dX(d, m_{\text{cat}}^*))\alpha_3 g}{1 - \alpha_1}. \quad (\text{D9})$$

If $\alpha_3 g \ll 1$, we find from this equation that m_{cat}^* can be expanded in powers of $\alpha_3 g$ as

$$m_{\text{cat}}^* = \frac{1 + A_1 \alpha_3 g + A_2 (\alpha_3 g)^2 + \dots}{\alpha_1 + \alpha_2}. \quad (\text{D10})$$

The coefficients are given by

$$A_1 = -1 + \frac{\alpha_2}{1 - \alpha_1} \left(1 - dX\left(d, \frac{1}{\alpha_1 + \alpha_2}\right)\right), \quad (\text{D11})$$

$$A_2 = -\frac{\alpha_2 d A_1}{(1 - \alpha_1)(\alpha_1 + \alpha_2)} \left. \frac{\partial X(d, m_{\text{cat}})}{\partial m_{\text{cat}}} \right|_{m_{\text{cat}}=1/(\alpha_1 + \alpha_2)}. \quad (\text{D12})$$

Substituting Eqs. (D8), and (D10) into Eq. (D6), we obtain the asymptotic behavior of μ^* as a function of $\alpha_3 g$ in the regime $\mu^* \ll \alpha_3 g \ll 1$ and $\mu^* \ll d$. Since m_{in}^* is proportional to $\alpha_3 g$, μ^* exhibits an essential singularity as $\alpha_3 g \rightarrow 0$, thereby justifying the assumption $\mu^* \ll \alpha_3 g$.

-
- [1] S. A. Kauffman, *The Origins of Order: Self-Organization and Selection in Evolution* (Oxford University Press, New York, NY, 1993).
- [2] K. Kaneko, *Life: an introduction to complex systems biology* (Springer, Berlin, Heidelberg, 2006).
- [3] K. Kaneko, *Universal Biology: The Physics of Life through the Macro-Micro Consistency Principle* (Cambridge University Press, Cambridge, 2025).
- [4] M. Ramirez-Gaona *et al.*, YMDB 2.0: a significantly expanded version of the yeast metabolome database, *Nucleic Acids Res.* **45**, D440–D445 (2016).
- [5] K. Haug *et al.*, Metabolights: a resource evolving in response to the needs of its scientific community, *Nucleic Acids Res.*, D440–D444 (2020).
- [6] D. S. Wishart *et al.*, HMDB 5.0: the human metabolome database for 2022, *Nucleic Acids Res.* **50**, D622–D631 (2022).
- [7] S. Kim *et al.*, Pubchem 2025 update, *Nucleic Acids Research* **53**, D1516–D1525 (2025).
- [8] M. Kanehisa, M. Furumichi, Y. Sato, Y. Matsuura, and M. Ishiguro-Watanabe, KEGG: biological systems database as a model of the real world, *Nucleic Acids Res.* **53**, D672–D677 (2025).
- [9] R. Albert and A.-L. Barabási, Statistical mechanics of complex networks, *Rev. Mod. Phys.* **74**, 47–97 (2002).
- [10] A.-L. Barabási and Z. N. Oltvai, Network biology: understanding the cell's functional organization, *Nat. Rev. Genet.* **5**, 101 (2004).
- [11] A.-L. Barabási, *Network Science* (Cambridge University Press, Cambridge, 2016).
- [12] H. Jeong, B. Tombor, R. Albert, Z. N. Oltvai, and A.-L. Barabási, The large-scale organization of metabolic networks, *Nature* **407**, 651–654 (2000).
- [13] H. Jeong, S. P. Mason, A.-L. Barabási, and Z. N. Oltvai, Lethality and centrality in protein networks, *Nature* **411**, 41–42 (2001).
- [14] A. Wagner and D. A. Fell, The small world inside large metabolic networks, *Proc. Biol. Sci.* **268**, 1803–1810 (2001).
- [15] E. Ravasz, A. L. Somera, D. A. Mongru, Z. N. Oltvai, and A.-L. Barabási, Hierarchical organization of modularity in metabolic networks, *Science* **297**, 1551–1555 (2002).
- [16] A. H. Y. Tong *et al.*, Global mapping of the yeast genetic interaction network, *Science* **303**, 808–813 (2004).
- [17] S. Li *et al.*, A map of the interactome network of the metazoan *C. elegans*, *Science* **303**, 540–543 (2004).
- [18] J. Nacher, T. Yamada, S. Goto, M. Kanehisa, and T. Akutsu, Two complementary representations of a scale-free network, *Physica A: Statistical Mechanics and its Applications* **349**, 349 (2005).
- [19] H. Ebel, L.-I. Mielsch, and S. Bornholdt, Scale-free topology of e-mail networks, *Phys. Rev. E* **66**, 035103 (2002).

- [20] E. Ferrara, A large-scale community structure analysis in facebook, *EPJ Data Sci.* **1**, 9 (2012).
- [21] J. Lin and Y. Ban, Complex network topology of transportation systems, *Transp. Rev.* **33**, 658 (2013).
- [22] T. Nesti, F. Sloothaak, and B. Zwart, Emergence of scale-free blackout sizes in power grids, *Phys. Rev. Lett.* **125**, 058301 (2020).
- [23] A.-L. Barabási, R. Albert, and H. Jeong, Scale-free characteristics of random networks: the topology of the world-wide web, *Physica A* **281**, 69 (2000).
- [24] R. Pastor-Satorras, A. Vázquez, and A. Vespignani, Dynamical and correlation properties of the internet, *Phys. Rev. Lett.* **87**, 258701 (2001).
- [25] R. Albert, H. Jeong, and A.-L. Barabási, Error and attack tolerance of complex networks, *Nature* **406**, 378 (2000).
- [26] R. Cohen, K. Erez, D. ben Avraham, and S. Havlin, Resilience of the internet to random breakdowns, *Phys. Rev. Lett.* **85**, 4626 (2000).
- [27] T. F. Cooper, A. P. Morby, A. Gunn, *et al.*, Effect of random and hub gene disruptions on environmental and mutational robustness in *Escherichia coli*, *BMC Genomics* **7**, 237 (2006).
- [28] R. Cohen and S. Havlin, *Complex networks: structure, robustness and function* (Cambridge university press, Cambridge, 2010).
- [29] O. Artime, M. Grassia, M. De Domenico, *et al.*, Robustness and resilience of complex networks, *Nat. Rev. Phys.* **6**, 114 (2024).
- [30] P. Oikonomou and P. Cluzel, Effects of topology on network evolution, *Nat. Phys.* **2**, 532–536 (2006).
- [31] S. F. Greenbury, I. G. Johnston, M. A. Smith, J. P. Doye, and A. A. Louis, The effect of scale-free topology on the robustness and evolvability of genetic regulatory networks, *Journal of Theoretical Biology* **267**, 48 (2010).
- [32] M. E. J. Newman, *Networks* (Oxford University Press, Oxford, 2010).
- [33] B. Barzel and A.-L. Barabási, Universality in network dynamics, *Nat. Phys.* **9**, 673–681 (2013).
- [34] S. N. Dorogovtsev, A. V. Goltsev, and J. F. F. Mendes, Critical phenomena in complex networks, *Rev. Mod. Phys.* **80**, 1275 (2008).
- [35] A. Aleksiejuk, J. A. Holyst, and S. D., Ferromagnetic phase transition in barabási-albert networks, *Physica A: Stat. Mech. Appl.* **310**, 260 (2002).
- [36] R. Pastor-Satorras and A. Vespignani, Epidemic spreading in scale-free networks, *Phys. Rev. Lett.* **86**, 3200 (2001).
- [37] K. Newton, A. Strasser, N. Kayagaki, and V. M. Dixit, Cell death, *Cell* **187**, 235 (2024).
- [38] Y. Himeoka, S. A. Horiguchi, and T. J. Kobayashi, Theoretical basis for cell deaths, *Phys. Rev. Research* **6**, 043217 (2024).
- [39] C. Furusawa and K. Kaneko, A dynamical-systems view of stem cell biology, *Science* **338**, 215–217 (2012).
- [40] R. Lanza and A. A., *Essentials of stem cell biology*, third edition ed. (Academic Press, Cambridge, Massachusetts, 2014).
- [41] C. Furusawa and K. Kaneko, Zipf’s law in gene expression, *Phys. Rev. Lett.* **90**, 088102 (2003).
- [42] H. R. Ueda, S. Hayashi, S. Matsuyama, T. Yomo, S. Hashimoto, S. A. Kay, J. B. Hogenesch, and M. Iino, Universality and flexibility in gene expression from bacteria to human, *Proc. Natl. Acad. Sci. U. S. A.* **101**, 3765–3769 (2004).
- [43] C. Lu and R. D. King, An investigation into the population abundance distribution of mRNAs, proteins, and metabolites in biological systems, *Bioinformatics* **25**, 2020–2027 (2009).
- [44] S. Sato, M. Horikawa, T. Kondo, T. Sato, and M. Setou, A power law distribution of metabolite abundance levels in mice regardless of the time and spatial scale of analysis, *Sci. Rep.* **8**, 10315 (2018).
- [45] S. Lazzardi, F. Valle, A. Mazzolini, A. Scialdone, M. Caselle, and M. Osella, Emergent statistical laws in single-cell transcriptomic data, *Phys. Rev. E* **107**, 044403 (2023).
- [46] C. Furusawa and K. Kaneko, Theory of robustness of irreversible differentiation in a stem cell system: Chaos hypothesis, *J. Theor. Biol.* **209**, 395 (2001).
- [47] C. Furusawa and K. Kaneko, Evolutionary origin of power-laws in a biochemical reaction network: Embedding the distribution of abundance into topology, *Phys. Rev. E* **73**, 011912 (2006).
- [48] C. Furusawa and K. Kaneko, Adaptation to optimal cell growth through self-organized criticality, *Phys. Rev. Lett.* **108**, 208103 (2012).
- [49] P. C. Martin, E. D. Siggia, and H. A. Rose, Statistical dynamics of classical systems, *Phys. Rev. A* **8**, 423–437 (1973).
- [50] H. Janssen, On a lagrangean for classical field dynamics and renormalization group calculations of dynamical critical properties, *Z. Phys. B* **23**, 377–380 (1976).
- [51] C. De Dominicis, Dynamics as a substitute for replicas in systems with quenched random impurities, *Phys. Rev. B* **18**, 4913–4919 (1978).
- [52] H. Sompolinsky and A. Zippelius, Relaxational dynamics of the edwards-anderson model and the mean-field theory of spin-glasses, *Phys. Rev. B* **25**, 6860–6875 (1982).
- [53] L. F. Cugliandolo and J. Kurchan, Analytical solution of the off-equilibrium dynamics of a long-range spin-glass model, *Phys. Rev. Lett.* **71**, 173–176 (1993).
- [54] T. Castellani and A. Cavagna, Spin-glass theory for pedestrians, *J. Stat. Mech.: Theory Exp.* **2005** (05), P05012.
- [55] T. Galla, Generating-functional analysis of random lotka-volterra systems: A step-by-step guide, *arXiv preprint arXiv:2405.14289* (2024).
- [56] K. Mimura and A. C. C. Coolen, Parallel dynamics of disordered ising spin systems on finitely connected directed random graphs with arbitrary degree distributions, *J. Phys. A: Math. Theor.* **42**, 415001 (2009).
- [57] L. Poley, T. Galla, and J. W. Baron, Interaction networks in persistent lotka-volterra communities, *Phys. Rev. E* **111**, 014318 (2025).
- [58] F. L. Metz, Dynamical mean-field theory of complex systems on sparse directed networks, *Phys. Rev. Lett.* **134**, 037401 (2025).
- [59] P. Erdős and A. Rényi, On random graphs I, *Publ. math. debrecen* **6**, 18 (1959).
- [60] S. N. Dorogovtsev, J. F. F. Mendes, and A. N. Samukhin, Structure of growing networks with preferential linking, *Phys. Rev. Lett.* **85**, 4633–4636 (2000).
- [61] B. Bollobás, A probabilistic proof of an asymptotic formula for the number of labelled regular graphs, *Eur. J. Combinatorics* **1**, 311–316 (1980).
- [62] F. Chung and L. Lu, Connected components in random graphs with given expected degree sequences, *Ann. Com-*

- binatorics **6**, 125–145 (2002).
- [63] M. Opper and S. Diederich, Phase transition and $1/\text{fnoise}$ in a game dynamical model, *Phys. Rev. Lett.* **69**, 1616–1619 (1992).
 - [64] W. H. Press, S. A. Teukolsky, W. T. Vetterling, and B. P. Flannery, *Numerical Recipes 3rd Edition: The Art of Scientific Computing*, 3rd ed. (Cambridge University Press, Cambridge, USA, 2007).
 - [65] B. Fotouhi and M. G. Rabbat, Degree correlation in scale-free graphs, *Eur. Phys. J. B* **86**, 510 (2013).
 - [66] T. Kaneko and M. Kikuchi, Evolution enhances mutational robustness and suppresses the emergence of a new phenotype: A new computational approach for studying evolution, *PLoS Comput. Biol.* **18**, e1009796 (2022).
 - [67] M. Kikuchi, Phenotype selection due to mutational robustness, *PLoS One* **19**, e0311058 (2024).

Supplementary Material for “Starvation suppression in scale-free metabolic networks: Dynamical mean-field analysis of dense catalytic reaction networks”

We consider a catalytic reaction network model consisting of N chemical species [41, 47]. The chemical species are divided into three groups: unpenetrable metabolic products, penetrable metabolic products, and nutrients, denoted by $\mathcal{G}_1, \mathcal{G}_2$ and \mathcal{G}_3 , respectively. The fractions of chemical species belonging to these groups are denoted by α_1, α_2 , and α_3 , respectively, satisfying $\alpha_1 + \alpha_2 + \alpha_3 = 1$. The model dynamics are described by the following differential equations:

$$\dot{x}_i(t) = \frac{1}{c} \sum_{j=1}^N \sum_{k \notin \mathcal{G}_3} C_{ij}^k x_j(t) x_k(t) - \frac{1}{c} \sum_{j=1}^N \sum_{k \notin \mathcal{G}_3} C_{ji}^k x_i(t) x_k(t) + d_i(g_i - x_i(t)) - \mu(t)x_i(t) + h_i(t) + \xi_i(t). \quad (\text{S1})$$

where the parameters (d_i, g_i) are defined as $(0, 0)$ for $i \in \mathcal{G}_1$, $(d, 0)$ for $i \in \mathcal{G}_2$, and (d, g) for $i \in \mathcal{G}_3$. $\mu = \frac{1}{N} \sum_{i=1}^N d_i(g_i - x_i)$ denotes the cell growth rate, and the term $-\mu(t)x_i(t)$ represents the dilution of chemical abundances due to the cell growth. The site-dependent field $h_i(t)$ is introduced for theoretical convenience and is set to zero at the end of the calculation. The variable $\xi_i(t)$ represents an uncorrelated Gaussian noise with zero mean and variance σ^2 (in the main text, we present results for $\xi_i(t) = 0$). The tensor C_{ij}^k is equal to 1 if the reaction $j + k \rightarrow i + k$ exists, and is equal to 0 otherwise. We suppose that the nutrients cannot act as catalysts, i.e., $C_{ij}^k = 0$ for all $k \in \mathcal{G}_3$. C_{ij}^k is generated using the configuration model [32, 62]. Specifically, we first draw the in-degree u_i , out-degree v_i , and catalytic degree w_i for all nodes i independently from the distributions $p_u^{(\text{in})}$, $p_v^{(\text{out})}$ and $p_w^{(\text{cat})}$. The probability distribution of C_{ij}^k is then given by

$$P(C_{ij}^k) = \frac{u_i v_j w_k}{(Nc)^2} \delta_{C_{ij}^k, 1} + \left(1 - \frac{u_i v_j w_k}{(Nc)^2}\right) \delta_{C_{ij}^k, 0}, \quad (\text{S2})$$

where c is the mean connectivity, i.e., $\lim_{N \rightarrow \infty} \frac{1}{N} \sum_{i,j,k} C_{ij}^k = \sum_u p_u^{(\text{in})} u = \sum_v p_v^{(\text{out})} v = (\alpha_1 + \alpha_2) \sum_w p_w^{(\text{cat})} w = c$.

We solve the dynamics of Eq. (S1) on a network generated by Eq. (S2) using dynamical mean-field theory [49–55]. The theory is based on the generating functional

$$\mathcal{Z}[\mathbf{h}, \boldsymbol{\psi}] = \int \left(\prod_{i=1}^N Dx_i \right) \mathcal{P}[\mathbf{x}, \mathbf{h}] e^{i \int dt \sum_{i=1}^N x_i(t) \psi_i(t)}. \quad (\text{S3})$$

The path probability distribution of \mathbf{x} can be written as

$$\mathcal{P}[\mathbf{x}, \mathbf{h}] = P_0(\mathbf{x}(0)) \int \left(\prod_{i=1}^N D\xi_i \right) \mathcal{P}_\sigma[\boldsymbol{\xi}] \quad (\text{S4})$$

$$\times \delta_{\text{F}} \left[\dot{x}_i(t) - \frac{1}{c} \sum_{j,k} C_{ij}^k x_j(t) x_k(t) + \frac{1}{c} \sum_{j',k'} C_{j'i}^{k'} x_{j'}(t) x_{k'}(t) - d_i(g_i - x_i(t)) + \mu(t)x_i(t) - h_i(t) - \xi_i(t) \right], \quad (\text{S5})$$

where $\mathcal{P}_\sigma[\boldsymbol{\xi}]$ is the path probability distribution of the Gaussian noise

$$\mathcal{P}_\sigma[\boldsymbol{\xi}] \sim \exp \left(-\frac{1}{2\sigma^2} \int dt \sum_{i=1}^N \xi_i^2(t) \right) \quad (\text{S6})$$

and $P_0(\mathbf{x}(0))$ represents the joint initial distribution for all nodes i . Using a functional integral representation of δ_{F} and integrating out the Gaussian noise $\boldsymbol{\xi}_i$, we obtain

$$\begin{aligned} \mathcal{Z}[\mathbf{h}, \boldsymbol{\psi}] = & \int \left(\prod_{i=1}^N Dx_i D\hat{x}_i \right) P_0(\mathbf{x}(0)) \exp \left(-\frac{i}{c} \sum_{i \neq j \neq k} C_{ij}^k \int dt \hat{x}_i(t) x_k(t) x_j(t) + \frac{i}{c} \sum_{i \neq j \neq k} C_{ji}^k \int dt \hat{x}_i(t) x_k(t) x_i(t) \right) \\ & \times \exp \left(i \int dt \sum_{i=1}^N A_i(x_i(t), \hat{x}_i(t), h_i(t), \psi_i(t)) \right), \quad (\text{S7}) \end{aligned}$$

where a single-site action is defined as

$$A_i(x_i(t), \hat{x}_i(t), h_i(t), \psi_i(t)) = x_i(t)\psi_i(t) + \frac{i\sigma^2}{2}\hat{x}_i^2(t) + \hat{x}_i(t)[\dot{x}_i(t) - d_i(g_i - x_i(t)) + \mu(t)x_i(t) - h_i(t)]. \quad (\text{S8})$$

From Eqs. (S7) and (S8), one finds that the fields $h_i(t)$ and $\psi_i(t)$ are coupled to the dynamical variables $\hat{x}_i(t)$ and $x_i(t)$, respectively. This leads to the following formulae,

$$\langle x_i(t) \rangle_\xi = (-i) \lim_{\mathbf{h}, \boldsymbol{\psi} \rightarrow 0} \frac{\delta Z[\mathbf{h}, \boldsymbol{\psi}]}{\delta \psi_i(t)}, \quad (\text{S9})$$

$$\langle \hat{x}_i(t) \rangle_\xi = i \lim_{\mathbf{h}, \boldsymbol{\psi} \rightarrow 0} \frac{\delta Z[\mathbf{h}, \boldsymbol{\psi}]}{\delta h_i(t)} = 0, \quad (\text{S10})$$

$$R(t_1, t_2) = \frac{1}{N} \sum_{i=1}^N \lim_{\boldsymbol{\psi} \rightarrow 0} \frac{\delta \langle x_i(t_2) \rangle_\xi}{\delta h_i(t_1)} = (-i) \lim_{\mathbf{h}, \boldsymbol{\psi} \rightarrow 0} \frac{1}{N} \sum_{i=1}^N \frac{\delta^n Z[\mathbf{h}, \boldsymbol{\psi}]}{\delta h_i(t_1) \delta \psi_i(t_2)} = \frac{-i}{N} \sum_{i=1}^N \langle \hat{x}_i(t_1) x_i(t_2) \rangle_\xi, \quad (\text{S11})$$

where $\langle \dots \rangle_\xi$ denotes the average over the noise and $R(t_1, t_2)$ represents the response function. Because of the causality, $R(t_1, t_2) = 0$ if $t_2 \leq t_1$, although $\lim_{t_2 \rightarrow t_1^-} R(t_1, t_2) \neq 0$. We also note that the generating functional satisfies the normalization condition $Z[\mathbf{h}, 0] = 1$, leading to $\langle \hat{x}_i(t) \rangle_\xi = 0$, as given in Eq. (S10).

Let us evaluate the generating functional $\overline{\mathcal{Z}[\mathbf{h}, \boldsymbol{\psi}]}$ averaged over the network topology $\{C_{ij}^k\}$. In general, this averaged generating functional can be written as

$$\overline{\mathcal{Z}[\mathbf{h}, \boldsymbol{\psi}]} = \int \left(\prod_{i=1}^N Dx_i D\hat{x}_i \right) P_0(\mathbf{x}(0)) \Delta[\mathbf{x}, \hat{\mathbf{x}}] \exp \left(i \int dt \sum_{i=1}^N A_i(x_i(t), \hat{x}_i(t), h_i(t), \psi_i(t)) \right), \quad (\text{S12})$$

where

$$\begin{aligned} \Delta[\mathbf{x}, \hat{\mathbf{x}}] &= \exp \left(-\frac{i}{c} \sum_{i \neq j \neq k} C_{ij}^k \int dt \hat{x}_i(t) x_k(t) x_j(t) + \frac{i}{c} \sum_{i \neq j \neq k} C_{ji}^k \int dt \hat{x}_i(t) x_k(t) x_i(t) \right) \\ &= \prod_{i \neq j \neq k} \exp \left(-\frac{i}{c} C_{ij}^k \int dt (\hat{x}_i(t) - \hat{x}_j(t)) x_k(t) x_j(t) \right) \\ &= \exp \left[\sum_{i \neq j \neq k} \ln \left(1 + \frac{u_i v_j w_k}{(Nc)^2} \left(\exp \left(-\frac{i}{c} \int dt (\hat{x}_i(t) - \hat{x}_j(t)) x_k(t) x_j(t) \right) - 1 \right) \right) \right] \end{aligned} \quad (\text{S13})$$

To decouple the interaction terms between different sites in $\Delta[\mathbf{x}, \hat{\mathbf{x}}]$, we introduce the following functional order parameters [56–58]:

$$U_{nu}[\hat{x}] = \frac{1}{\alpha_n p_u^{(\text{in})} N} \sum_{i \in \mathcal{G}_n} \delta_{u_i, u} \delta_{\text{F}}[\hat{x}(t) - \hat{x}_i(t)] \quad (n = 1, 2, 3), \quad (\text{S14})$$

$$V_{nv}[x, \hat{x}] = \frac{1}{\alpha_n p_v^{(\text{out})} N} \sum_{i \in \mathcal{G}_n} \delta_{v_i, v} \delta_{\text{F}}[x(t) - x_i(t)] \delta_{\text{F}}[\hat{x}(t) - \hat{x}_i(t)] \quad (n = 1, 2, 3), \quad (\text{S15})$$

$$W_{nw}[x] = \frac{1}{\alpha_n p_w^{(\text{cat})} N} \sum_{i \in \mathcal{G}_n} \delta_{w_i, w} \delta_{\text{F}}[x(t) - x_i(t)] \quad (n = 1, 2). \quad (\text{S16})$$

For notational convenience, we also introduce $W_{3w}[x] = 0$. Using these order parameters, we can write $\Delta[\mathbf{x}, \hat{\mathbf{x}}]$ as

$$\Delta[\mathbf{x}, \hat{\mathbf{x}}] = \exp \left[N \sum_{u, v, w} p_u^{(\text{in})} p_v^{(\text{out})} p_w^{(\text{cat})} \int D\hat{x} Dy D\hat{y} Dz \left(\sum_{n=1}^3 \alpha_n U_{nu}[\hat{x}] \right) \left(\sum_{n=1}^3 \alpha_n V_{nv}[y, \hat{y}] \right) \left(\sum_{n=1}^3 \alpha_n W_{nw}[z] \right) f_{uv}^w[\hat{x}, y, \hat{y}, z] \right], \quad (\text{S17})$$

where

$$f_{uv}^w[\hat{x}, y, \hat{y}, z] = N^2 \ln \left(1 + \frac{uvw}{(Nc)^2} \left(\exp \left(-\frac{i}{c} \int dt (\hat{x}(t) - \hat{y}(t)) y(t) z(t) \right) - 1 \right) \right). \quad (\text{S18})$$

In the dense connectivity limit, the leading terms in powers of $1/c$ are relevant. Hence, by expanding the exponential in Eq. (S18) with respect to $1/c$ and taking the thermodynamic limit $N \rightarrow \infty$ and, we obtain

$$f_{uv}^w[\hat{x}, y, \hat{y}, z] = -i \frac{uvw}{c^3} \int dt (\hat{x}(t) - \hat{y}(t)) y(t) z(t). \quad (\text{S19})$$

By inserting the following identities,

$$\begin{aligned} 1 &= \int DU_{nu} \delta_{\text{F}} \left[\alpha_n p_u^{(\text{in})} N U_{nu}[\hat{x}] - \sum_{i \in \mathcal{G}_n} \delta_{u_i, u} \delta_{\text{F}}[\hat{x}(t) - \hat{x}_i(t)] \right] \\ &= \frac{1}{2\pi} \int DU_{nu} D\hat{U}_{nu} e^{i\alpha_n p_u^{(\text{in})} N \int D\hat{x} \hat{U}_{nu}[\hat{x}] U_{nu}[\hat{x}] - i \sum_{i \in \mathcal{G}_n} \delta_{u_i, u} \hat{U}_{nu}[\hat{x}_i]}, \end{aligned} \quad (\text{S20})$$

$$\begin{aligned} 1 &= \int DV_{nv} \delta_{\text{F}} \left[\alpha_n p_v^{(\text{out})} N V_{nv}[x, \hat{x}] - \sum_{i \in \mathcal{G}_n} \delta_{v_i, v} \delta_{\text{F}}[x(t) - x_i(t)] \delta_{\text{F}}[\hat{x}(t) - \hat{x}_i(t)] \right] \\ &= \frac{1}{2\pi} \int DV_{nv} D\hat{V}_{nv} e^{i\alpha_n p_v^{(\text{out})} N \int Dx D\hat{x} \hat{V}_{nv}[x, \hat{x}] V_{nv}[x, \hat{x}] - i \sum_{i \in \mathcal{G}_n} \delta_{v_i, v} \hat{V}_{nv}[x_i, \hat{x}_i]}, \end{aligned} \quad (\text{S21})$$

$$\begin{aligned} 1 &= \int DW_{nw} \delta_{\text{F}} \left[\alpha_n p_w^{(\text{cat})} N W_{nw}[x] - \sum_{i \in \mathcal{G}_n} \delta_{w_i, w} \delta_{\text{F}}[x(t) - x_i(t)] \right] \\ &= \frac{1}{2\pi} \int DW_{nw} D\hat{W}_{nw} e^{i\alpha_n p_w^{(\text{cat})} N \int Dx \hat{W}_{nw}[x] W_{nw}[x] - i \sum_{i \in \mathcal{G}_n} \delta_{w_i, w} \hat{W}_{nw}[x_i]}, \end{aligned} \quad (\text{S22})$$

into the averaged generating functional $\overline{\mathcal{Z}[\mathbf{h}, \boldsymbol{\psi}]}$, We obtain

$$\overline{\mathcal{Z}[\mathbf{h}, \boldsymbol{\psi}]} = \int \left(\prod_{n,u} DU_{nu} D\hat{U}_{nu} \right) \left(\prod_{n,v} DV_{nv} D\hat{V}_{nv} \right) \left(\prod_{n,w} DW_{nw} D\hat{W}_{nw} \right) \exp\left(N\Phi[\mathbf{U}, \hat{\mathbf{U}}, \mathbf{V}, \hat{\mathbf{V}}, \mathbf{W}, \hat{\mathbf{W}}]\right), \quad (\text{S23})$$

where

$$\begin{aligned} \Phi &= \sum_{u,v,w} p_u^{(\text{in})} p_v^{(\text{out})} p_w^{(\text{cat})} \int D\hat{x} Dy D\hat{y} Dz \left(\sum_{n=1}^3 \alpha_n U_{nu}[\hat{x}] \right) \left(\sum_{n=1}^3 \alpha_n V_{nv}[y, \hat{y}] \right) \left(\sum_{n=1}^3 \alpha_n W_{nw}[z] \right) f_{uv}^w[\hat{x}, y, \hat{y}, z] \\ &+ i \sum_{n=1}^3 \alpha_n \left(\sum_u p_u^{(\text{in})} \int D\hat{x} U_{nu}[\hat{x}] \hat{U}_{nu}[\hat{x}] + \sum_v p_v^{(\text{out})} \int Dx D\hat{x} V_{nv}[x, \hat{x}] \hat{V}_{nv}[x, \hat{x}] + \sum_w p_w^{(\text{cat})} \int Dx W_{nw}[x] \hat{W}_{nw}[x] \right) \\ &+ \sum_{n,u,v,w} \alpha_n p_u^{(\text{in})} p_v^{(\text{out})} p_w^{(\text{cat})} \ln \left(\int Dx D\hat{x} P_0(x(0)) \right. \\ &\quad \left. \times \exp \left[i \int dt A_n(x(t), \hat{x}(t), h_{nuv}^w(t), \psi_{nuv}^w(t)) - i \hat{U}_{nu}[\hat{x}] - i \hat{V}_{nv}[x, \hat{x}] - i \hat{W}_{nw}[x] \right] \right). \end{aligned} \quad (\text{S24})$$

Here, we assume that $h_i(t)$ and $\psi_i(t)$ depend only on the in-degree u , out-degree v , catalytic degree w and group \mathcal{G}_n of the i -th chemical species; this assumption leads to the factorized form of the last term in Eq. (S24).

The integral in Eq. (S23) can be evaluated by applying the saddle-point method in the large N limit, and then the

resulting saddle-point equations read

$$\hat{U}_{nu}[\hat{x}] = i \sum_{v,w} p_v^{(\text{out})} p_w^{(\text{cat})} \int Dy D\hat{y} Dz \left(\sum_{n=1}^3 \alpha_n V_{nv}[y, \hat{y}] \right) \left(\sum_{n=1}^3 \alpha_n W_{nw}[z] \right) f_{uv}^w[\hat{x}, y, \hat{y}, z] \equiv \hat{U}_u[\hat{x}], \quad (\text{S25})$$

$$\hat{V}_{nv}[y, \hat{y}] = i \sum_{u,w} p_u^{(\text{in})} p_w^{(\text{cat})} \int D\hat{x} Dz \left(\sum_{n=1}^3 \alpha_n U_{nu}[\hat{x}] \right) \left(\sum_{n=1}^3 \alpha_n W_{nw}[z] \right) f_{uv}^w[\hat{x}, y, \hat{y}, z] \equiv \hat{V}_v[y, \hat{y}], \quad (\text{S26})$$

$$\hat{W}_{nw}[z] = i \sum_{u,v} p_u^{(\text{in})} p_v^{(\text{out})} \int D\hat{x} Dy D\hat{y} \left(\sum_{n=1}^3 \alpha_n U_{nu}[\hat{x}] \right) \left(\sum_{n=1}^3 \alpha_n V_{nv}[y, \hat{y}] \right) f_{uv}^w[\hat{x}, y, \hat{y}, z] \equiv \hat{W}_w[z], \quad (\text{S27})$$

$$U_{nu}[\hat{x}] = \sum_{v,w} p_v^{(\text{out})} p_w^{(\text{cat})} \int Dx \gamma[x, \hat{x}|n, u, v, w], \quad (\text{S28})$$

$$V_{nv}[y, \hat{y}] = \sum_{u,w} p_v^{(\text{out})} p_w^{(\text{cat})} \gamma[y, \hat{y}|n, u, v, w], \quad (\text{S29})$$

$$W_{nw}[z] = \sum_{u,v} p_u^{(\text{in})} p_v^{(\text{out})} \int D\hat{z} \gamma[z, \hat{z}|n, u, v, w], \quad (\text{S30})$$

where

$$\gamma[x, \hat{x}|n, u, v, w] = \frac{\exp \left[i \int dt A_n(x(t), \hat{x}(t), h_{nuv}^w(t), \psi_{nuv}^w(t)) - i \hat{U}_u[\hat{x}] - i \hat{V}_v[x, \hat{x}] - i \hat{W}_w[x] \right]}{\int Dx D\hat{x} \exp \left[i \int dt A_n(x(t), \hat{x}(t), h_{nuv}^w(t), \psi_{nuv}^w(t)) - i \hat{U}_u[\hat{x}] - i \hat{V}_v[x, \hat{x}] - i \hat{W}_w[x] \right]}. \quad (\text{S31})$$

It should be noted that the saddle-point equations for the conjugate (hatted) order parameters do not depend on the species group n ; therefore, we introduce the shorthand notation, $\hat{U}_u[\hat{x}]$, $\hat{V}_v[y, \hat{y}]$, and $\hat{W}_w[z]$.

To interpret the probability distribution $\gamma[x, \hat{x}|n, u, v, w]$, we define the expectation with respect to $\gamma[x, \hat{x}|n, u, v, w]$ as

$$\langle \cdots \rangle_{nuv}^w = \int Dx D\hat{x} \cdots \gamma[x, \hat{x}|n, u, v, w]. \quad (\text{S32})$$

By calculating the functional derivatives of the expression for the generating functional $\overline{\mathcal{Z}[\mathbf{h}, \boldsymbol{\psi}]}$ in Eq. (S23) with respect to $\psi_{nuv}^w(t)$ and $h_{nuv}^w(t)$, we find the following relations:

$$\begin{aligned} \langle x(t) \rangle_{nuv}^w &= \int Dx D\hat{x} x(t) \gamma[x, \hat{x}|n, u, v, w] = (-i) \lim_{\mathbf{h}, \boldsymbol{\psi} \rightarrow 0} \frac{\delta \overline{\mathcal{Z}[\mathbf{h}, \boldsymbol{\psi}]}}{\delta \psi_{nuv}^w(t)} \\ &= (-i) \lim_{\mathbf{h}, \boldsymbol{\psi} \rightarrow 0} \frac{1}{\alpha_n p_u^{(\text{in})} p_v^{(\text{out})} p_w^{(\text{cat})} N} \sum_{i \in \mathcal{G}_n} \delta_{u_i, u} \delta_{v_i, v} \delta_{w_i, w} \frac{\delta \overline{\mathcal{Z}[\mathbf{h}, \boldsymbol{\psi}]}}{\delta \psi_i(t)} \\ &= \frac{1}{\alpha_n p_u^{(\text{in})} p_v^{(\text{out})} p_w^{(\text{cat})} N} \sum_{i \in \mathcal{G}_n} \delta_{u_i, u} \delta_{v_i, v} \delta_{w_i, w} \langle x_i(t) \rangle_{\xi}, \end{aligned} \quad (\text{S33})$$

$$\begin{aligned} \langle \hat{x}(t) \rangle_{nuv}^w &= \int Dx D\hat{x} \hat{x}(t) \gamma[x, \hat{x}|n, u, v, w] = i \lim_{\mathbf{h}, \boldsymbol{\psi} \rightarrow 0} \frac{\delta \overline{\mathcal{Z}[\mathbf{h}, \boldsymbol{\psi}]}}{\delta h_{nuv}^w(t)} \\ &= i \lim_{\mathbf{h}, \boldsymbol{\psi} \rightarrow 0} \frac{1}{\alpha_n p_u^{(\text{in})} p_v^{(\text{out})} p_w^{(\text{cat})} N} \sum_{i \in \mathcal{G}_n} \delta_{u_i, u} \delta_{v_i, v} \delta_{w_i, w} \frac{\delta \overline{\mathcal{Z}[\mathbf{h}, \boldsymbol{\psi}]}}{\delta h_i(t)} \\ &= \frac{1}{\alpha_n p_u^{(\text{in})} p_v^{(\text{out})} p_w^{(\text{cat})} N} \sum_{i \in \mathcal{G}_n} \delta_{u_i, u} \delta_{v_i, v} \delta_{w_i, w} \langle \hat{x}_i(t) \rangle_{\xi} = 0, \end{aligned} \quad (\text{S34})$$

$$\langle x(t) \hat{x}(t') \rangle_{nuv}^w = \int Dx D\hat{x} x(t) \hat{x}(t') \gamma[x, \hat{x}|n, u, v, w] = \frac{1}{\alpha_n p_u^{(\text{in})} p_v^{(\text{out})} p_w^{(\text{cat})} N} \sum_{i \in \mathcal{G}_n} \delta_{u_i, u} \delta_{v_i, v} \delta_{w_i, w} \langle x(t) \hat{x}_i(t') \rangle_{\xi}. \quad (\text{S35})$$

Comparing these relations with Eqs. (S9-S11), one can regard $\int Dx D\hat{x} \gamma[x, \hat{x}|n, u, v, w]$ as the path probability describing the typical dynamics of the abundance of the chemical species belonging to \mathcal{G}_n , conditioned on the in-degree u ,

out-degree v , and catalytic degree w . Using Eqs. (S33-S35) and substituting Eqs. (S19, S28-S30) into Eq. (S27), we find

$$\begin{aligned} \hat{W}_w[z] &= \sum_{u,v} p_u^{(\text{in})} p_v^{(\text{out})} \frac{uvw}{c^3} \left[\int dt \left(\sum_{n=1}^3 \alpha_n \sum_{v',w'} p_{v'}^{(\text{out})} p_{w'}^{(\text{cat})} \langle \hat{x}(t) \rangle_{nuv'}^{w'} \right) \left(\sum_{n=1}^3 \alpha_n \sum_{v',w'} p_{v'}^{(\text{in})} p_{w'}^{(\text{cat})} \langle y(t) \rangle_{nu'v}^{w'} \right) z(t) \right. \\ &\quad \left. - \left(\sum_{n=1}^3 \alpha_n \sum_{u',w'} p_{u'}^{(\text{in})} p_{w'}^{(\text{cat})} \langle y(t) \hat{y}(t) \rangle_{nu'v}^{w'} \right) z(t) \right] \\ &= 0. \end{aligned} \quad (\text{S36})$$

Here, we use $\langle \hat{x}(t) \rangle_{nuv}^w = 0$ and $\langle \hat{x}(t)x(t) \rangle_{nuv}^w = 0$. Vanishing of $\hat{W}_w[z]$ implies that $\int D\hat{x} \gamma[x, \hat{x}|n, u, v, w]$ does not depend on the catalytic degree w , i.e., the effective dynamics of the chemical abundance is independent of w . This result has a clear physical interpretation. The catalyzed chemical species do not provide feedback to the catalytic chemical species through the catalytic activity. Thus, the number of catalytic links w does not affect the effective dynamics of the chemical abundance and then the probability measure and averages can be simplified as $\gamma[x, \hat{x}|n, u, v, w] \rightarrow \gamma[x, \hat{x}|n, u, v]$ and $\langle \cdots \rangle_{nuv}^w \rightarrow \langle \cdots \rangle_{nuv}$.

Similarly to $\hat{W}_w[z]$, the other hatted order parameters can be calculated as

$$\begin{aligned} \hat{U}_u[\hat{x}] &= \sum_{v,w} p_v^{(\text{out})} p_w^{(\text{cat})} \frac{uvw}{c^3} \left[\int dt \hat{x}(t) \left(\sum_{n=1}^3 \alpha_n \sum_{u'} p_{u'}^{(\text{in})} \langle y(t) \rangle_{nu'v} \right) \left(\sum_{n=1}^2 \alpha_n \sum_{u',v'} p_{u'}^{(\text{in})} p_{v'}^{(\text{out})} \langle z(t) \rangle_{nu'v'} \right) \right. \\ &\quad \left. - \left(\sum_{n=1}^3 \alpha_n \sum_{u'} p_{u'}^{(\text{in})} \langle \hat{y}(t)y(t) \rangle_{nu'v} \right) \left(\sum_{n=1}^2 \alpha_n \sum_{u',v'} p_{u'}^{(\text{in})} p_{v'}^{(\text{out})} \langle z(t) \rangle_{nu'v'} \right) \right] \\ &= \frac{u}{c} \int dt \hat{x}(t) m_{\text{in}}(t) m_{\text{cat}}(t), \end{aligned} \quad (\text{S37})$$

$$\begin{aligned} \hat{V}_v[y, \hat{y}] &= \sum_{u,w} p_u^{(\text{in})} p_w^{(\text{cat})} \frac{uvw}{c^3} \left[\int dt \left(\sum_{n=1}^3 \alpha_n \sum_{v'} p_{v'}^{(\text{out})} \langle \hat{x}(t) \rangle_{nuv'} \right) y(t) \left(\sum_{n=1}^2 \alpha_n \sum_{u',v'} p_{u'}^{(\text{in})} p_{v'}^{(\text{out})} \langle z(t) \rangle_{nu'v'} \right) \right. \\ &\quad \left. - \hat{y}(t)y(t) \left(\sum_{n=1}^2 \alpha_n \sum_{u',v'} p_{u'}^{(\text{in})} p_{v'}^{(\text{out})} \langle z(t) \rangle_{nu'v'} \right) \right] \\ &= -\frac{v}{c} \int dt \hat{y}(t)y(t) m_{\text{cat}}(t), \end{aligned} \quad (\text{S38})$$

where

$$m_{\text{in}}(t) = \sum_{n,u,v} \frac{v}{c} \alpha_n p_u^{(\text{in})} p_v^{(\text{out})} \langle x(t) \rangle_{nuv}, \quad (\text{S39})$$

$$m_{\text{cat}}(t) = \frac{\sum_{u,v} p_u^{(\text{in})} p_v^{(\text{out})} (\alpha_1 \langle x(t) \rangle_{1uv} + \alpha_2 \langle x(t) \rangle_{2uv})}{\alpha_1 + \alpha_2}. \quad (\text{S40})$$

Substituting Eqs. (S37) and (S38) into $\gamma[x, \hat{x}|n, u, v]$, we obtain

$$\gamma[x, \hat{x}|n, u, v] = \frac{\exp \left[i \int dt A_n(x(t), \hat{x}(t), h_{nuv}(t), \psi_{nuv}(t)) - i \hat{x}(t) \left(\frac{u}{c} m_{\text{in}}(t) m_{\text{cat}}(t) - \frac{v}{c} x(t) m_{\text{cat}}(t) \right) \right]}{\int Dx D\hat{x} \exp \left[i \int dt A_n(x(t), \hat{x}(t), h_{nuv}(t), \psi_{nuv}(t)) - i \hat{x}(t) \left(\frac{u}{c} m_{\text{in}}(t) m_{\text{cat}}(t) - \frac{v}{c} x(t) m_{\text{cat}}(t) \right) \right]}. \quad (\text{S41})$$

The path probability of the effective dynamical equation for the abundance of the chemical species belonging to \mathcal{G}_n , conditioned on the in-degree u and out-degree v , can then be written as

$$\begin{aligned} \mathcal{P}[x_{nuv}, h_{nuv}] &= P_0(x_{nuv}(0)) \int D\xi_{nuv} \mathcal{P}_\sigma[\xi_{nuv}] \\ &\quad \times \delta_{\text{F}} \left[\dot{x}_{nuv}(t) - \frac{u}{c} m_{\text{in}}(t) m_{\text{cat}}(t) + \frac{v}{c} m_{\text{cat}}(t) x_{nuv}(t) - d_n (g_n - x_{nuv}(t)) + \mu(t) x_{nuv}(t) - h_{nuv}(t) - \xi_{nuv}(t) \right]. \end{aligned} \quad (\text{S42})$$

Hence, we finally obtain the effective dynamical equations as

$$\dot{x}_{nuv}(t) = \frac{u}{c} m_{\text{in}}(t) m_{\text{cat}}(t) - \frac{v}{c} m_{\text{cat}}(t) x_{nuv}(t) + d_n (g_n - x_{nuv}(t)) - \mu(t) x_{nuv}(t) + h_{nuv}(t) + \xi_{nuv}(t). \quad (\text{S43})$$

In the main text, we analyze the case of $h_{nuv}(t) = \xi_{nuv}(t) = 0$.